NASA TECHNICAL NOTE

NASA TN D-3931

NASA TN D-3931

COOLDOWN CHARACTERISTICS OF REGENERATIVE NOZZLE USED IN FULL-SCALE, COLD-FLOW, NUCLEAR ROCKET TEST FACILITY

by George E. Turney and Eileen Cox

Lewis Research Center

Cleveland, Ohio

NATIONAL AERONAUTICS AND SPACE ADMINISTRATION • WASHINGTON, D. C. • MAY 1967

NASA TN D-3931

COOLDOWN CHARACTERISTICS OF REGENERATIVE NOZZLE USED IN FULL-SCALE, COLD-FLOW, NUCLEAR ROCKET TEST FACILITY

By George E. Turney and Eileen Cox

Lewis Research Center
Cleveland, Ohio

NATIONAL AERONAUTICS AND SPACE ADMINISTRATION

For sale by the Clearinghouse for Federal Scientific and Technical Information
Springfield, Virginia 22151 – CFSTI price $3.00

COOLDOWN CHARACTERISTICS OF REGENERATIVE NOZZLE USED IN FULL-SCALE, COLD-FLOW, NUCLEAR ROCKET TEST FACILITY

by George E. Turney and Eileen Cox

Lewis Research Center

SUMMARY

An analytical and experimental study was made of the transient pressure-drop - heat-transfer characteristics of a regeneratively cooled nozzle assembly used in startup tests conducted with a full-scale, unfueled, nuclear rocket simulation system.

The pressure drops and heat-transfer rates with gaseous, two-phase, and subcooled liquid hydrogen flow in the nozzle assembly were computed and compared with experimental measurements.

The experimental and calculated results show that the time constant for the chilldown of the nozzle is extremely small. For the startup test run presented herein, the coolant-tube temperatures near the nozzle tube inlet were reduced from approximately 510° to 50° R in the first 4 seconds of the startup transient.

For the most part, the calculated and measured temperatures of the nozzle coolant tubes exhibited similar trends. Except for local inflections in some of the measured temperatures (caused by unstable two-phase boiling), the calculated material temperatures for the convergent segment of the nozzle tubes were within, or reasonably near, the experimental accuracy of the measured material temperatures. The largest relative differences in predicted and measured local coolant-tube temperatures occurred at locations on the divergent length of the nozzle tubes during the two-phase-flow and liquid-flow periods of the test run.

The calculated and measured static pressure drops in the nozzle tubes were in reasonably close agreement throughout most of the test run. However, during the time span in which the two-phase hydrogen flow mixture was predominately liquid, the calculated pressure drops were considerably larger than the measured values. A possible explanation of this difference is that the Martinelli relations, which were used in the pressure-drop analysis, tend to overestimate the frictional loss for two-phase hydrogen flow, particularly when the two-phase flow mixture is predominately liquid.

INTRODUCTION

The application of nuclear power for rocket propulsion requires the ability to analytically predict the heat-transfer rates and pressure drops in the individual components of the nuclear propulsion system during all phases of propulsion system operation.

The three principal phases of operation as related to a nuclear rocket propulsion system are (1) system chilldown associated with the reactor startup transient, (2) steady-state design power operation, and (3) system shutdown and decay heat removal operation. Of these three principal operating phases, the startup transient is traversed the most rapidly and, as such, would be expected to result in rapid changes in the temperature of particular components in the nuclear rocket system.

In order to investigate the startup characteristics of a full-scale nuclear rocket propulsion system and obtain information needed to predict individual component and overall system performance during a nuclear rocket startup, a series of test runs was made with the B-1, full-scale, nuclear rocket simulation system located at the Plum Brook Station of the Lewis Research Center. A detailed description of the B-1, full-scale test facility and the system turbopump and a comparison of analytical and experimental turbopump data are presented in reference 1. The startup test runs conducted in the B-1 facility were of a nonnuclear nature; that is, the reactor core used in these flow experiments was unfueled. Consequently, the thermal energy transferred to the hydrogen propellant flowing in the system was derived from the sensible heat of the flow-system components.

The information obtained from the B-1, full-scale tests is intended to provide experimental information to be used as guidelines for evaluating heat transfer and pressure drop correlations used by digital and analog computer programs for predicting individual component performance and overall system performance during a startup. Heat-transfer, pressure-drop, and flow characteristics of the regeneratively cooled nozzle assembly used in the B-1, full-scale, cold-flow tests are described herein. The nozzle assembly used in these tests is described in detail in the APPARATUS AND EXPERIMENTAL PROCEDURE section of this report.

The analysis of the regeneratively cooled nozzle assembly is complicated by the fact that gaseous, two-phase, and subcooled liquid-hydrogen flow occur in the nozzle coolant tubes during a startup transient. In the early part of the startup, the hydrogen flow entering the nozzle coolant passages is gaseous at low pressure and temperature. As the chilldown progresses, the hydrogen entering the nozzle coolant passages changes to a two-phase-flow mixture (gas-liquid) and eventually to a subcooled liquid.

Because of the unusual physical properties of hydrogen, it appears that the standard techniques used in the correlation of boiling data for common liquids (e.g., water, petroleum oils, etc.) may not be applicable to the forced convective boiling of two-phase or liquid hydrogen.

For the low values of wall-to-bulk temperature difference anticipated in the nozzle coolant passages during a startup transient, the heat-transfer rates with two-phase or liquid-hydrogen flow may differ considerably depending on the mechanism of convective boiling. The possible uncertainty in the heat-transfer mechanism (nucleate boiling or

film boiling) inside the coolant tubes could have a significant effect on the estimated heat-transfer rates and pressure drops in the nozzle tubes during a startup. The criterion used to analytically estimate the mechanism of convective boiling of hydrogen during a startup transient is described in the ANALYTICAL PROCEDURE section of this report.

The experimental pressure-drop and heat-transfer data of two typical B-1 test runs (liquid-hydrogen runs 19 and 24) were compared with analytically predicted values for the regeneratively cooled nozzle assembly. In general, the experimental and analytical chilldown data for these two test runs exhibited similar trends. Because of this similarity, only the data of liquid-hydrogen test run 24 are presented in this report.

The results of liquid-hydrogen test run 24 along with the assumptions, equations, and analytical procedures used to predict the pressure-drop - heat-transfer characteristics are presented herein. The quasi-steady-state equations of pressure drop and heat transfer used in the transient analysis were programed for and solved on a digital computer; a brief description of the digital computer code and the analytical methods of computation is also included.

In order to predict the pressure-drop - heat-transfer characteristics of the regeneratively cooled nozzle assembly, the following preliminary assumptions were made:

(1) The hydrogen temperature, pressure, density, and flow rate are the same in each of the parallel coolant passages of the nozzle assembly.

(2) Quasi-steady-state equations may be used to adequately predict the transient chilldown characteristics of the nozzle assembly.

(3) A single-passage flow model (single nozzle coolant tube) gives an adequate representation of the nozzle assembly during the startup transient.

Although the reactor core used in the B-1, full-scale tests was unfueled, the chilldown characteristics of this system are considered to be representative of the initial time period (approximately the first 15 sec) in the startup phase of the typical nuclear rocket prototype system.

APPARATUS AND EXPERIMENTAL PROCEDURE

Research System

Figure 1 shows the B-1 test stand and associated components. The research system, that is, the full-scale, cold-flow test system, is located inside the B-1 test stand enclosure and consists of a propellant storage tank, turbopump, reactor, and nozzle in an assembled configuration, as shown in figure 2.

The propellant storage tank mounted near the top of the test stand has a 2000-gallon

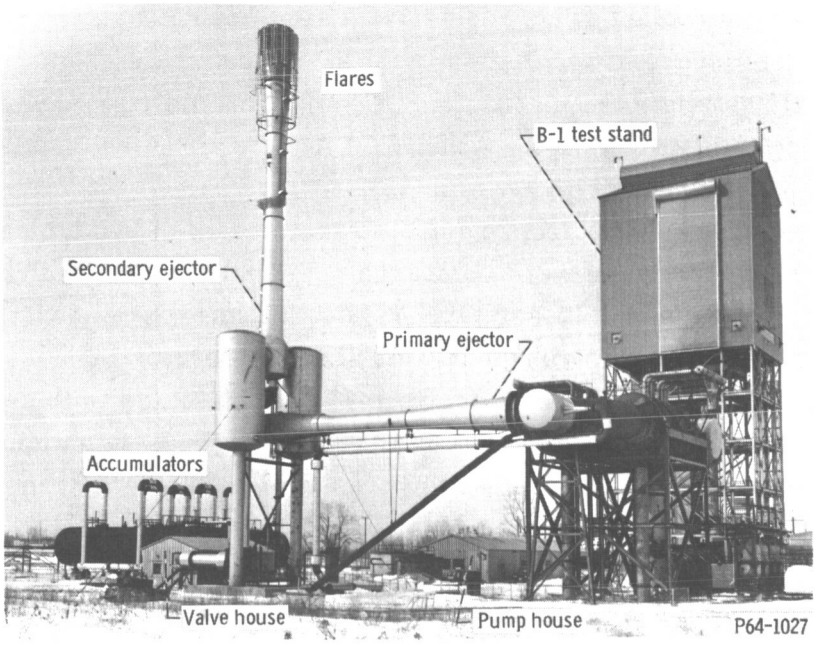

Figure 1. - B-1 test stand and associated components.

capacity. The storage tank has a 4-inch-thick covering of polyurethane insulation. The outlet at the bottom of the storage tank is connected to the turbopump by an $8\frac{1}{2}$-foot-long section of 8-inch-diameter pipe; this section of pipe contains a turbine flowmeter and two 8-inch butterfly valves. A 4-inch-nominal-diameter propellant feedline (approximately 18 ft long) connects the pump outlet to the nozzle inlet manifold. Downstream of the pump outlet in the propellant feedline is a venturi flowmeter and a servo-operated main valve. The propellant feedline is heavily instrumented and is covered with foam-in-place insulation.

The terminal end of the 4-inch-diameter propellant feedline is branched into three parallel flowlines, which are connected to three equally spaced ports on the nozzle inlet manifold. The regeneratively cooled nozzle is mounted directly underneath a modified KIWI B-1B reactor assembly. The reactor core assembly used in these tests contained unfueled graphite modules; the modified KIWI B-1B reactor assembly is described in detail in reference 2.

The side reflector assembly used in the B-1 engine system contained fixed control drums and dummy control drum actuators.

The hydrogen propellant entering the nozzle inlet manifold flows upward through the parallel coolant tubes and into the reflector inlet plenum. The flow then continues through the reflector passages and into the dome cavity above the reactor core, where the flow is folded (flow direction is reversed) and passed downward through the reactor core and nozzle and into the altitude exhaust system.

The altitude exhaust system on which the nozzle is mounted is partly evacuated by a

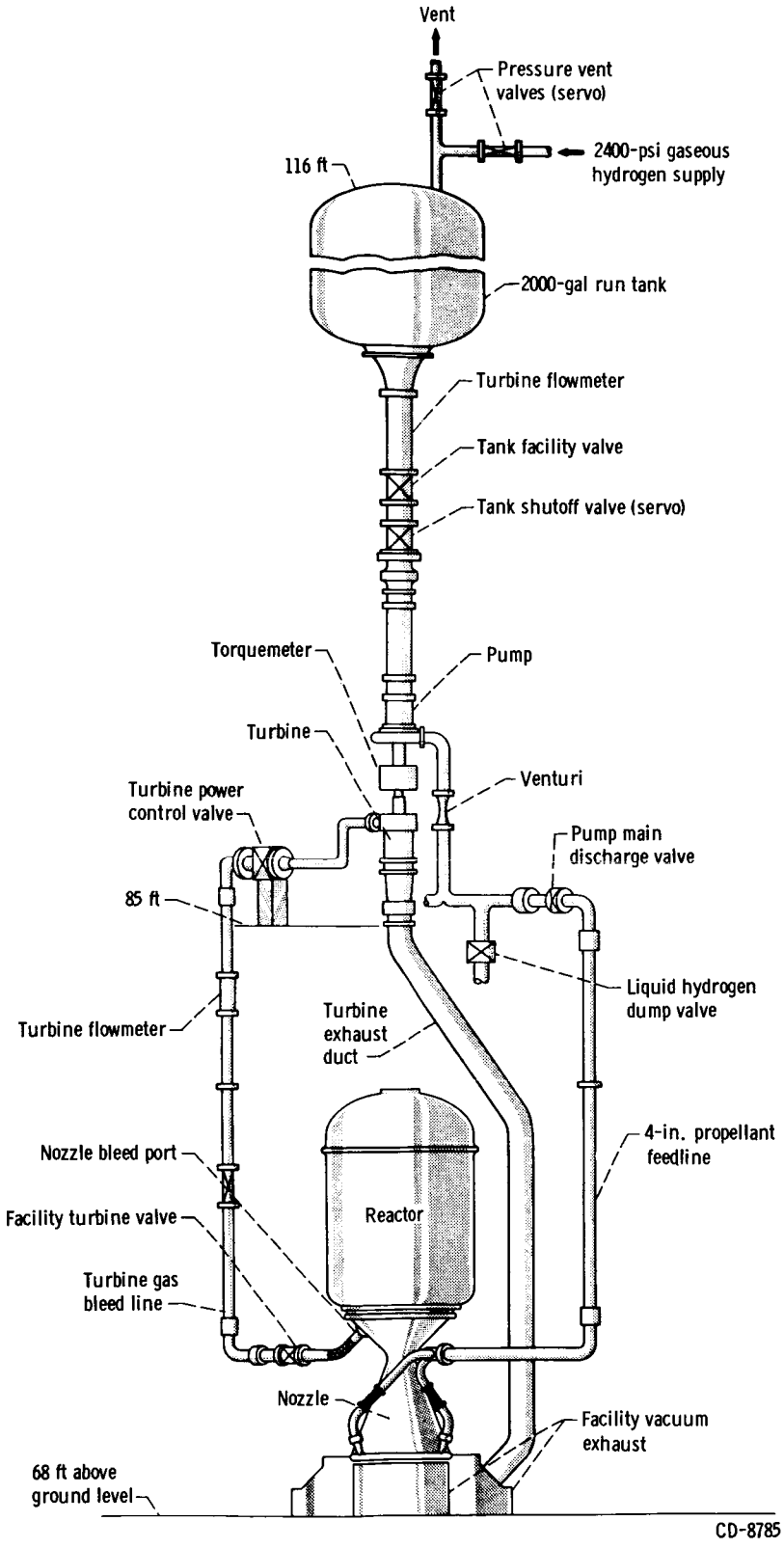

Figure 2. - Full-scale, cold-flow test system.

two-stage, steam-driven ejector system that simulates the nozzle exhaust back pressure levels anticipated at flight conditions.

The overall experimental assembly just described is a reasonable simulation of a full-scale, flight-type, nuclear rocket engine assembly.

Nozzle Assembly

The regeneratively cooled tubular-wall nozzle assembly used in the B-1 cold-flow engine system is shown in figure 3. This nozzle, designated RN-2 serial number 005, was fabricated by the Rocketdyne Division of North American Aviation and has a contraction ratio of 17.3 to 1, an expansion ratio of 12 to 1, and an axial length of 58.02 inches.

The RN-2 nozzle assembly consists of a tubular-wall construction, fabricated from 180 geometrically similar coolant tubes. The hydrogen coolant enters the nozzle inlet manifold through three parallel flowlines and flows upward through the nozzle coolant tubes.

The formed and tapered tubes are made of Inconel-X and have a constant wall thick-

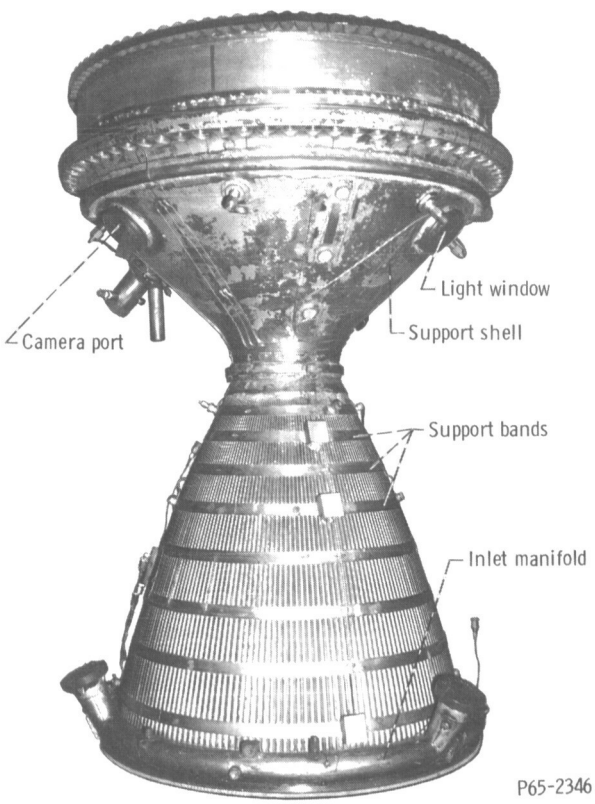

Figure 3. - Photograph of RN-2 nozzle assembly used in B-1 system tests.

ness of 0.009 inch. The cross-sectional shape of the nozzle coolant tubes is octagonal over a major portion of the tube length. In the vicinity of the nozzle throat, the cross-sectional shape is approximately elliptical.

The convergent portion of the coolant-tube assembly is covered by a continuous Inconel-X support shell that is brazed to the individual coolant tubes. The thickness of the support shell varies from a minimum value of 0.22 inch at the nozzle throat to maximum value of 0.28 inch at the nozzle chamber inlet. A total of eight support bands made of Inconel-X surround the outer surface of the coolant tubes in the divergent region of the nozzle.

The RN-2 nozzle assembly used in the B-1, cold-flow tests had been subjected to testing with chemical propellants (heat-flux simulation tests) prior to being instrumented and installed in the B-1 test stand. These previous high-temperature tests resulted in transverse thermal buckling and transverse cracking of the tubes on the hot gas side of the nozzle. Some of these tube failures were repaired by means of saddle patching. Not all of the leaks, however, were sealed. Because this nozzle was to be used in the B-1 facility for cold-flow startup tests, soft solder was used to repair the accessible leaks. Leaks in the coolant tubes between the pressure shell and tubes were discovered but could not be repaired. Consequently, a manifold was welded to the pressure shell, and the leakage was collected in the manifold and vented to the altitude exhaust system.

The hydrogen leakage from the nozzle tubes was estimated to be relatively small. Results from pressurized water tests indicated that the hydrogen leakage rate was less than 0.25 percent of the total flow rate in the nozzle assembly.

Instrumentation

Each of the major components of the B-1 research system was extensively instrumented; approximately 875 separate items of instrumentation were installed on the research system. The locations of the pressure and temperature measurements recorded for the nozzle assembly and referred to herein are shown in figure 4.

The pressures in the nozzle were measured with calibrated strain-gage-type transducers. Nozzle material temperatures were measured with fine-wire (30-gage) copper-constantan thermocouples. The details of typical thermocouple and static pressure tap installations are depicted in figure 5.

Since the outside face of the nozzle coolant tubes in the chamber region was covered with a support shell, thermocouples used to measure the coolant-tube wall temperatures in this region were positioned on the face of the coolant tubes, which is contacted by the gas flowing in the nozzle chamber. In the divergent region, thermocouple-measuring junctions were positioned on both the inside and the outside faces of the nozzle. The

PRESSURE MEASUREMENTS

Item designation	Axial distance from nozzle throat, x, in.	Reference angle, θ, deg	Tube number	Range, psia
Coolant Tubes				
NP-11	-29.3	185	93	0 to 200
NP-10	-19.6	↓	↓	↓
NP-9	0			
NP-8	13.2			
NP-7	22.2			
Nozzle Inlet Manifold				
NP-1	-----	45	---	0 to 200
NP-3	-----	185	---	0 to 200
Nozzle Exhaust Side				
NP-50	13.2	140	---	0 to 100
NP-39	0	26	---	0 to 100
NP-42	-29.3	32	---	0 to 100

TEMPERATURE MEASUREMENTS

Item designation	Axial distance from nozzle throat, x, in.	Reference angle, θ, deg	Tube number	Side[a]	Radial distance from nozzle axis, ℛ, in.
Coolant Tubes					
NT-90	-27.3	355	178	o	----
NT-89	-23.3	↓	↓	o	----
NT-30	-19.6			i	----
NT-32	-19.6			o	----
NT-88	-14.8			o	----
NT-31	-10.3			o	----
NT-87	-5.3			o	----
NT-27	6.6			i	----
NT-26	13.2			i	----
NT-86	-27.3	185	93	o	----
NT-14	-19.6	↓	↓	o	----
NT-80	-14.8			o	----
NT-13	-10.3			o	----
NT-11	-10.3			i	----
NT-10	0			i	----
NT-9	6.6			i	----
NT-7	22.2			i	----
NT-82	-27.3	45	23	o	----
NT-80	-14.8	↓	↓	o	----
NT-79	-5.3			o	----
NT-19	6.6			i	----
NT-17	22.2			i	----
Fluid Temperature at Inlet Manifold					
NR-1	-----	45	---	--	----
NR-2	-----	115	---	--	----
NR-4	-----	235	---	--	----
Fluid Temperature at Nozzle Chamber					
NT-60	22.2	22	---	--	11.5
NT-61	↓	22	---	--	5.5
NT-62		202	---	--	.5
NT-63		202	---	--	5.5
NT-64		202	---	--	11.5
Nozzle Support-Shell Surface					
NT-39	13.2	185	---	--	----
NT-40	6.6	185	---	--	----

[a]i(inside) refers to nozzle tube surface facing chamber axis; o(outside) refers to nozzle tube surface facing away from chamber axis.

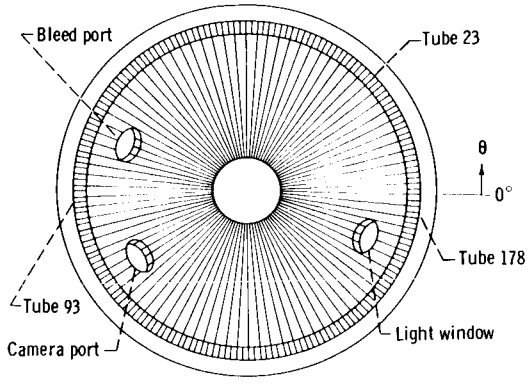

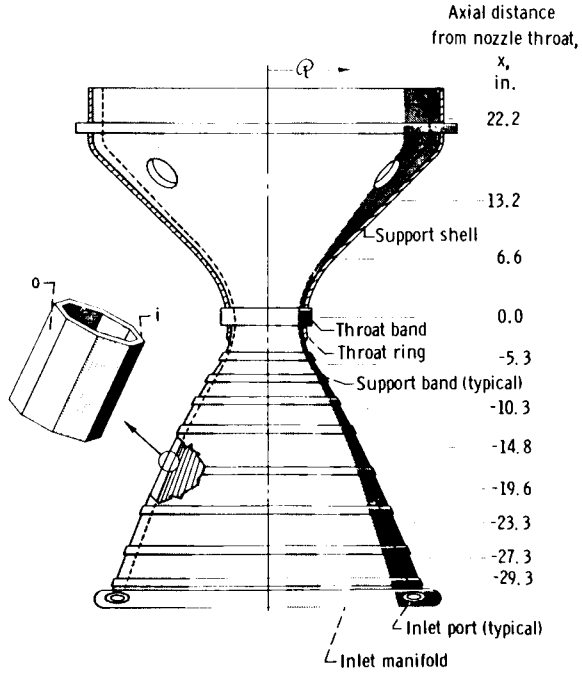

Figure 4. - RN-2 nozzle instrumentation.

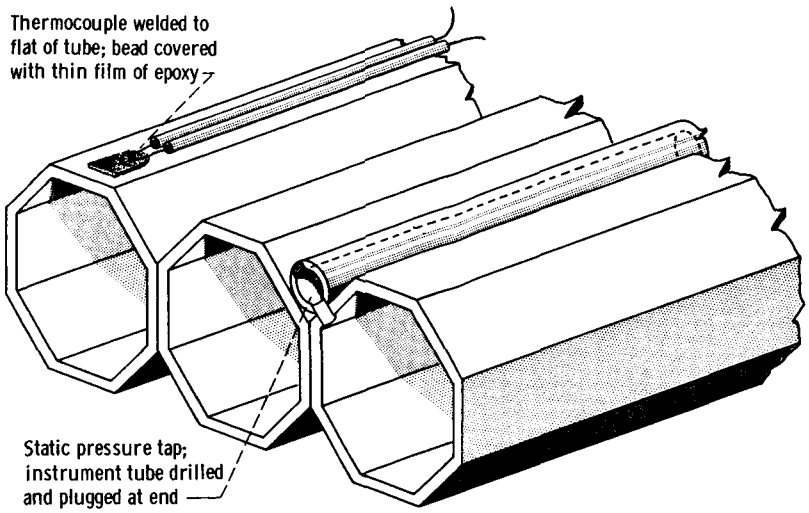

Figure 5. - Typical pressure and thermocouple installations on nozzle tubes.

location of thermocouple-measuring junctions with respect to the nozzle faces is indicated in figure 4 where i (inside) refers to the portion of the tube surface that is contacted by the gas in the nozzle chamber, and o (outside) refers to the portion of the tube surface that is furthest from the chamber gas stream. (All symbols are defined in appendix A.)

The prefixes on the item numbers tabulated in figure 4 designate the types of sensing elements used for the specific measurements. The item number prefixes, along with their respective designations, are as follows:

Item number prefix	Nozzle measurement	Type of sensor
NT	Temperature	Copper-constantan thermocouple
NP	Pressure	Pressure transducer
NR	Temperature	Resistance-type temperature sensor

The coolant tubes in the nozzle assembly are systematically numbered starting with tube 1 at a reference angle θ of 0^{o}. For the two test runs analyzed, experimental measurements were taken on only 3 of the 180 tubes in the assembly. The location of these tubes (tubes 23, 93, and 178) relative to the three ports on the nozzle chamber is depicted in figure 4.

In order to minimize heat input to the outside of the nozzle from the surrounding atmosphere, the entire nozzle assembly was covered with a $1\frac{1}{2}$-inch thickness of glass-fiber insulation.

Measurements of the hydrogen flow rate were taken at three different points in the B-1 engine system. The liquid-hydrogen flow from the storage tank was measured with a calibrated turbine flowmeter installed in the 8-inch line directly downstream of the tank outlet. A venturi flowmeter (located in the 4-inch line downstream of the pump) was used as a backup for measuring the hydrogen flow rate from the storage tank.

Experimental measurements of fluid temperature and pressure in the chamber of the nozzle were used to compute the flow rate of gaseous hydrogen at the outlet of the system. The computed values of flow rate through the nozzle were based on the assumptions that the flow is isentropically accelerated through the nozzle and that the Mach number at the exhaust nozzle throat is unity. The equations used to compute the flow rates through the nozzle are given in reference 2.

Data Acquisition and Processing

The digital and analog data acquisition equipment used in the B-1 engine system tests is described in reference 2. All temperature and pressure measurements on the nozzle assembly were recorded on digital equipment. Two different digital systems were used to record test data; 100 selected channels of data were recorded on a 10-kilocycle digital system, and 192 channels of data were recorded on a 4-kilocycle digital system. The individual channels were recorded at frequencies of 100 samples per second for the 10-kilocycle system and 20.86 samples per second for the 4-kilocycle system.

The recorded digital data were edited and checked for possible anomalies prior to being processed. Data channels that were found to have erroneous readings were deleted from the lists. The raw data were then processed on a digital computer, which converted the millivolt values to engineering units of temperature and pressure. The recorded data were averaged by using a 7-sample group for the 4-kilocycle system and a 10-sample group for the 10-kilocycle system. As a result of the group-averaging technique, the converted experimental values of temperature and pressure were printed out by the computer at frequencies of 10 values per second for the 10-kilocycle system and 2.98 values per second for the 4-kilocycle system.

Precision of Experimental Data

A discussion of the estimated accuracies of the experimental measurements and a description of possible errors introduced into the data by the acquisition system and processing methods are presented in reference 2.

The precision of measured pressures in the nozzle assembly was estimated to be

within ±1 percent of the full-scale pressure transducer range. The ranges of the individual transducers used for pressure measurements on the RN-2 nozzle assembly are tabulated in figure 4. The accuracy of pressures measured in the inlet manifold and nozzle coolant tubes (where 0 to 200 psia transducers were used) was estimated to be within ±2 pounds per square inch. In the nozzle chamber (where 0 to 100 psia transducers were used), the accuracy of the pressure measurements was estimated to be within ±1 pound per square inch.

Based on pretest calibrations with liquid hydrogen, the accuracy of the flow rate determinations made with the turbine meter was estimated to be within $\pm 2\frac{1}{2}$ percent of the actual flow rate. The accuracy of the flow-rate measurements made with the exhaust nozzle is somewhat uncertain; it is generally believed, however, to be in the neighborhood of ±4 percent of the actual flow rate through the nozzle.

Flow rates at different points in the system were determined by subtracting the estimated rates of flow accumulation in the upstream piping from the measured flow rates at the inlet to the system. The equations and procedure used to evaluate the flow rates at the inlet to the nozzle coolant tubes are given in reference 3.

Temperatures on the nozzle assembly were measured with copper-constantan thermocouples and resistance-type sensors. The precision of the individual temperature measurements is dependent on both the type of sensor and the temperature range in which the measurements are made. The National Bureau af Standards specifications for copper-constantan thermocouples in the range of 200° to -300° F include an estimated precision of $\pm 0.75^{\circ}$ F for 200° to -75° F and an estimated precision of ±1 percent of measured values for -75° to -300° F (ref. 4).

The accuracy of temperature measurements made with copper-constantan thermocouples below -300° F (160° R) is difficult to access. In the range from -300° F (160° R) to -430° F (30° R), the sensitivity of copper-constantan is relatively small. (Sensitivity as used here is the change in the thermoelectric potential with change in temperature.) In the liquid-hydrogen temperature region, the sensitivity of copper-constantan is only about one-tenth that at room temperature. As a result, measurements made with copper-constantan in the liquid-hydrogen temperature regime are appreciably affected by such factors as the resolution of the data recording system, variations in the thermoelectric powers of different wire pairs, and line noise in the data acquisition system. For the B-1 system, the errors associated with measurements made with copper-constantan in the liquid-hydrogen temperature region were estimated to be as great as $\pm 15^{\circ}$ R. The temperature measurements made with resistance-type sensors were estimated to be accurate to within about $\pm 2^{\circ}$ R.

In addition to the inaccuracies associated with these temperature-measuring devices, time lags (particularly during periods of rapid temperature changes) may also influence the recorded temperature values.

Of all the time-dependent variables in the B-1 system, probably the most difficult to accurately determine is the fluid quality, The computed values of hydrogen quality entering the nozzle inlet manifold and used in the analysis herein were determined from an energy balance on the system. The methods and procedure used in the quality determinations are described in reference 3. Because of possible nonequilibrium conditions in the two-phase hydrogen flow, no definite estimates were made of the accuracy of the calculated fluid qualities.

Test Operation

The experimental procedure used in the operation of the B-1 test facility is described in reference 1. The following is a summary of this procedure together with a brief description of the processes occurring in the system during a typical chilldown run.

Prior to the initiation of a test run, the facility is checked out and prepared for operation. The prerun procedures consist of electronic calibrations of the instrumentation, evacuation and helium purge of the entire system, filling of the liquid-hydrogen storage tank, and a prerun chilldown of the turbopump assembly.

The experimental run procedure begins with evacuation of the facility exhaust system by the flow of steam through the exhaust ejectors. When the exhaust system reaches a preset pressure level (usually 3 psia), a sequencer control circuit is engaged, which automatically regulates the operations required to obtain the desired run conditions.

When the required startup conditions are reached, flow of hydrogen from the storage tank is initiated by a programed opening of the control valve in the flow line downstream of the turbopump discharge. Time zero (τ_0) corresponds to the initiation of flow by opening the flow control valve.

As liquid hydrogen flows from the propellant tank through the feedline to the nozzle, it is gradually vaporized. In the early portion of the startup, gaseous hydrogen at low pressure and temperature enters the nozzle coolant tubes. As flow continues, the temperatures of the propellant feed line and nozzle coolant tubes continually decrease with time. As the chilldown progresses, less hydrogen is evaporated in the propellant feedline and, as a result, a larger fraction of the hydrogen entering the nozzle coolant tubes is in the liquid phase.

Simultaneously with the chilldown transient, the bootstrapping turbopump is started, causing a continuing increase of pressure and flow of the hydrogen entering the nozzle coolant passages. Consequently, during the chilldown, vaporization of hydrogen with the associated two-phase-flow heat transfer and pressure drop takes place in a highly dynamic condition throughout the coolant passages of the nozzle. With increasing time, the temperature of the engine system is lowered and, as a result, liquid and two-phase

hydrogen flow occur throughout the major portion of the engine system.

In the full-scale hot tests, for example, the hot tests run in the ROVER program, the reactor power is programed to increase as the chilldown progresses and, hence, prevents liquid or two-phase hydrogen from entering the reactor core. In the B-1 system tests, the startup simulation was considered to end at a time when two-phase hydrogen flow entered the reactor core.

ANALYTICAL PROCEDURE

Nozzle Analytical Code (NAC)

A quasi-steady-state computer code, Nozzle Analytical Code (NAC), was written and assembled to analyze the pressure-drop - heat-transfer characteristics of the regeneratively cooled RN-2 nozzle assembly used in the B-1 engine system tests. The specific objectives of the code, as related to the B-1 engine system chilldown tests, are (1) to predict the material temperatures of the nozzle as a function of time and axial position and (2) to predict the temperature, pressure, and quality of the coolant (hydrogen) in the nozzle assembly as a function of time and axial position.

A significant portion of the logic and calculational procedure used in the program is applicable only to the RN-2 nozzle geometry. With some internal modifications, however, NAC could be used to predict the thermodynamic performance of flowing hydrogen in other nozzle assemblies.

NAC is capable of computing the pressure-drop - heat-transfer characteristics of the nozzle for gaseous, two-phase, and liquid-hydrogen flow conditions. The hydrogen physical properties and transport properties used in the computer program were obtained from the digital function subroutine described in reference 5. A description of the single-passage flow model used to represent the nozzle assembly is presented in this section.

Flow model. - In formulating a model for the RN-2 nozzle assembly, the coolant-tube assembly was considered to be made up of two major longitudinal segments of lengths L_1 and L_2, as shown in figure 6. The length L_1 represents that segment of the nozzle extending from the nozzle inlet manifold to the nozzle throat; length L_2 represents that segment of the nozzle that extends from the nozzle throat to the coolant-tube outlet and is supported on the outside surface by the structural shell. Each of the major segments (L_1 and L_2) of the single-tube flow model was divided into a number of subsegments (herein referred to as stages) of equal length. For the analysis, a flow-stage length of 2.0 inches was used, which resulted in a total of 32 flow stages to represent the overall nozzle coolant-tube length. (The curvilinear length of the RN-2

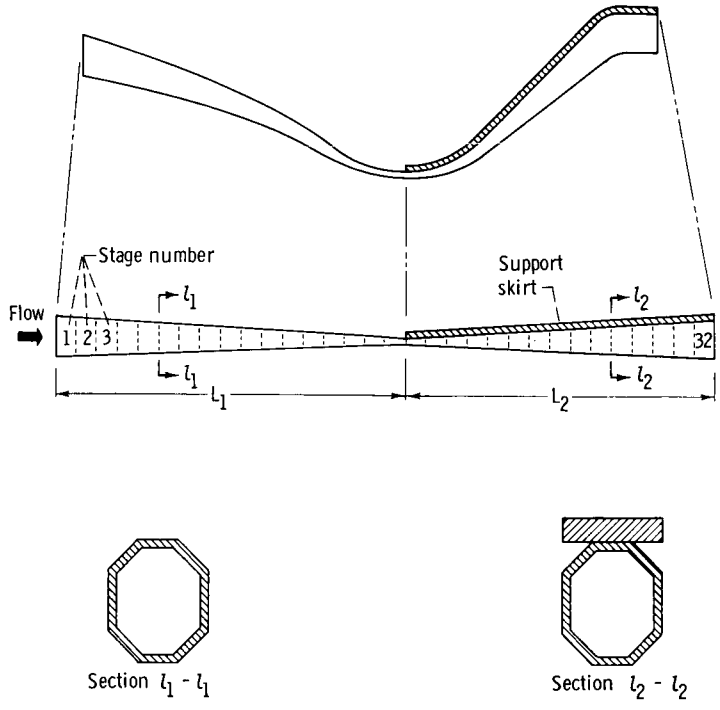

Figure 6. - Single-tube flow model representing RN-2 nozzle assembly.

nozzle coolant tubes was determined to be 64 in.)

The flow model shown in figure 6 is an axisymmetric, convergent-divergent flow passage. Cross sections of the two major segments of the single-tube flow model are also shown in figure 6. As indicated in this figure, the length of the axisymmetric flow model is equivalent to the curvilinear length of an RN-2 coolant tube. The flow stages that compose the model are numbered consecutively starting with flow stage 1 at the coolant-tube inlet and continuing through to flow stage 32 at the coolant-tube outlet. The inlet to flow stage 18 corresponds to the nozzle throat.

The use of a single-passage flow model to represent the RN-2 nozzle assembly is justified on the basis of the assumption that the temperatures, pressures, fluid densities, and flow rates in the individual coolant tubes are identical at each point in time throughout a transient chilldown test run. As a result of the assumption of uniform flow in the nozzle coolant tubes, the flow rate in the single-tube flow model $\dot{\omega}_c$ is related to the total nozzle flow rate $\dot{\omega}_{tot}$ by

$$\dot{\omega}_c = \frac{\dot{\omega}_{tot}}{180} \tag{1}$$

The portion of the nozzle assembly that is supported by the Inconel-X support shell was analyzed by considering the flow stages in that segment of the nozzle (segment L_2)

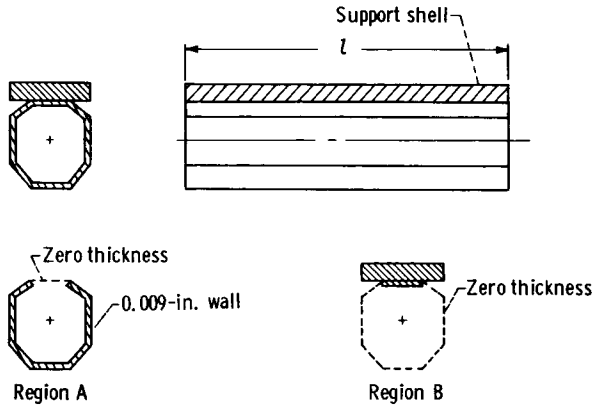

Figure 7. - Typical flow stage in segment L_2 of single-tube flow model.

to be made up of two separate regions, as shown in figure 7.

In separating the individual flow stages of segment L_2 into two regions (A and B), it was assumed that heat transfer by conduction from region B to region A was negligible during a transient chilldown of the nozzle. As a result of this assumption, an adiabatic boundary was imposed at the connection of the two regions.

The validity of this assumption was investigated analytically for a range of conditions typical of those expected during a transient chilldown of the nozzle assembly. The results of this investigation showed that (1) the heat interchange by conduction from region B to region A during a chilldown was small in relation to the heat transferred by convection across the coolant-tube fluid film boundary and (2) the average material temperatures of the two regions were only slightly affected by neglecting the heat transferred by conduction across the boundary connecting the two regions.

A brief description of the procedure used in the NAC for predicting the pressure drops and heat-transfer rates in the RN-2 nozzle assembly is presented in the next section. The equations and methods of solution employed in the analysis are dependent on the type of flow (gas, two-phase, or liquid-hydrogen flow) and the segment of the nozzle being analyzed. A more detailed description of the NAC is presented in appendix B.

Flow diagram. - Figure 8 is a simplified flow diagram of the NAC. The program is started by reading in three groups of input data. The time-dependent input data (group III) consists of a list of time-dependent values for each input variable. The values of each variable in the list correspond to a specific time period in the time span of a test run.

Starting at time zero τ_0 and considering the initial time period $\tau_1 - \tau_0$, the values of each time-dependent variable together with the initial temperatures of the coolant tubes and support shell (material temperatures at τ_0) are entered in the program. As indicated in figure 8, the equations used in the pressure-drop - heat-transfer analysis are dependent on the quality of the hydrogen entering the nozzle coolant tubes. In describing the calculational procedure used in the NAC, the flow at the inlet to flow stage 1 is considered to be in the gaseous state, that is, $X_{1,in} = 1.0$. (The general procedure used in the gas flow subroutine and two-phase and liquid flow subroutine is similar.) Calculations begin with flow stage 1 using the appropriate input values for the initial time period.

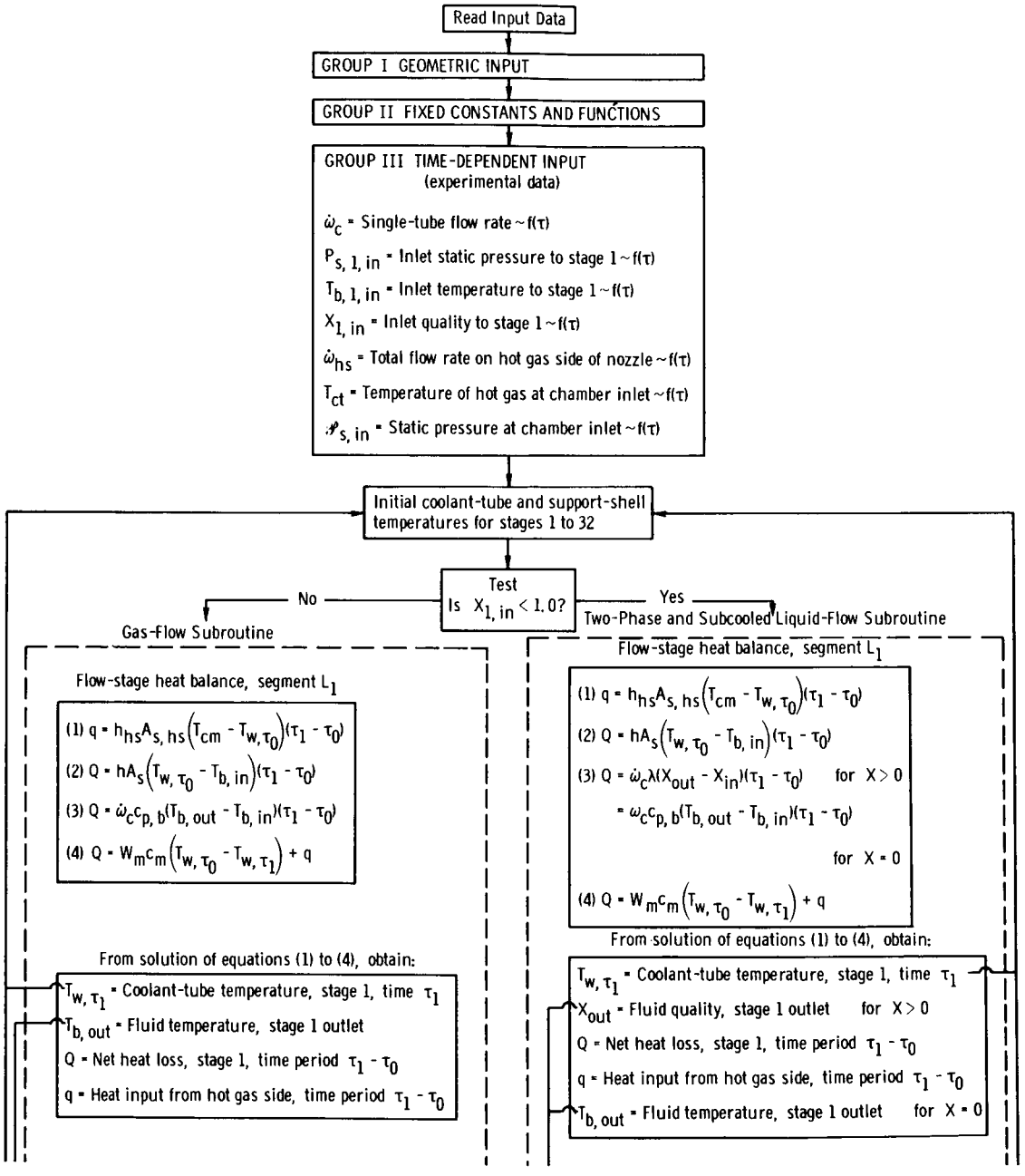
Read Input Data
GROUP I GEOMETRIC INPUT
GROUP II FIXED CONSTANTS AND FUNCTIONS
GROUP III TIME-DEPENDENT INPUT
(experimental data)
$\dot{\omega}_c$ = Single-tube flow rate ~ f(τ)
$P_{s,1,in}$ = Inlet static pressure to stage 1 ~ f(τ)
$T_{b,1,in}$ = Inlet temperature to stage 1 ~ f(τ)
$X_{1,in}$ = Inlet quality to stage 1 ~ f(τ)
$\dot{\omega}_{hs}$ = Total flow rate on hot gas side of nozzle ~ f(τ)
T_{ct} = Temperature of hot gas at chamber inlet ~ f(τ)
$P_{s,in}$ = Static pressure at chamber inlet ~ f(τ)
Initial coolant-tube and support-shell temperatures for stages 1 to 32
Test
Is $X_{1,in} < 1.0$?
No
Yes
Gas-Flow Subroutine
Two-Phase and Subcooled Liquid-Flow Subroutine
Flow-stage heat balance, segment L_1
(1) $q = h_{hs}A_{s,hs}\left(T_{cm} - T_{w,\tau_0}\right)(\tau_1 - \tau_0)$
(2) $Q = hA_s\left(T_{w,\tau_0} - T_{b,in}\right)(\tau_1 - \tau_0)$
(3) $Q = \dot{\omega}_c c_{p,b}(T_{b,out} - T_{b,in})(\tau_1 - \tau_0)$
(4) $Q = W_m c_m\left(T_{w,\tau_0} - T_{w,\tau_1}\right) + q$
From solution of equations (1) to (4), obtain:
T_{w,τ_1} = Coolant-tube temperature, stage 1, time τ_1
$T_{b,out}$ = Fluid temperature, stage 1 outlet
Q = Net heat loss, stage 1, time period $\tau_1 - \tau_0$
q = Heat input from hot gas side, time period $\tau_1 - \tau_0$
Flow-stage heat balance, segment L_1
(1) $q = h_{hs}A_{s,hs}\left(T_{cm} - T_{w,\tau_0}\right)(\tau_1 - \tau_0)$
(2) $Q = hA_s\left(T_{w,\tau_0} - T_{b,in}\right)(\tau_1 - \tau_0)$
(3) $Q = \dot{\omega}_c\lambda(X_{out} - X_{in})(\tau_1 - \tau_0)$ for $X > 0$
$= \omega_c c_{p,b}(T_{b,out} - T_{b,in})(\tau_1 - \tau_0)$
for $X = 0$
(4) $Q = W_m c_m\left(T_{w,\tau_0} - T_{w,\tau_1}\right) + q$
From solution of equations (1) to (4), obtain:
T_{w,τ_1} = Coolant-tube temperature, stage 1, time τ_1
X_{out} = Fluid quality, stage 1 outlet for $X > 0$
Q = Net heat loss, stage 1, time period $\tau_1 - \tau_0$
q = Heat input from hot gas side, time period $\tau_1 - \tau_0$
$T_{b,out}$ = Fluid temperature, stage 1 outlet for $X = 0$

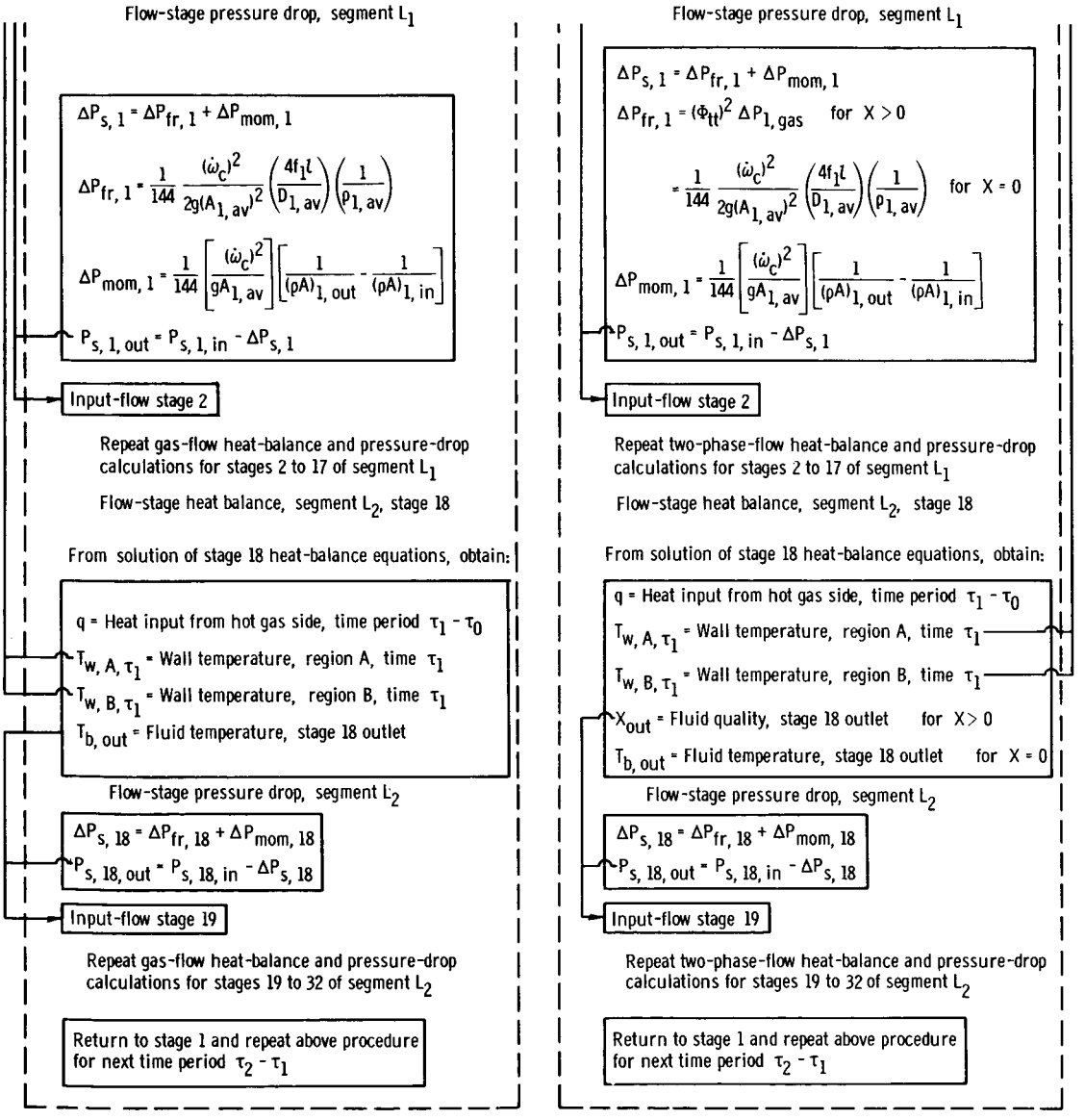

Figure 8. - Simplified flow diagram of NAC.

The fluid temperature at the stage 1 outlet $T_{b,out}$ and the average material temperature of stage 1 at τ_1, which is T_{w,τ_1}, are obtained by an iterative solution of the heat-balance equations for stage 1. Next, the static pressure at the flow stage 1 outlet $P_{s,1,out}$ is determined by computing the stage 1 static pressure drop $\Delta P_{s,1}$ and subtracting this pressure drop from the inlet pressure. The stage 1 outlet conditions $P_{s,1,out}$ and $T_{b,out}$ are then used as the inlet conditions to stage 2. The procedure just described, in which calculated outlet conditions of temperature and pressure for a flow stage are used as inlet conditions for the following stage, is repeated for each stage in the single-tube flow model.

The stepwise procedure used to compute outlet fluid conditions and material temperatures for the flow stages in segment L_2, that is, stages 18 to 32, is similar to that used for segment L_1. In segment L_2, however, average material temperatures for regions A and B of each stage are obtained along with the values of static pressure and fluid temperature at the outlet of each flow stage.

When the analysis of all flow stages in the first time period $\tau_1 - \tau_0$ is completed, the computed values (results) are stored and/or printed out by the computer. The calculated material temperatures at the end of the first time period are then assigned to the respective stages as initial conditions for the second time period $\tau_2 - \tau_1$. The time-dependent input for the second time period is then read into the program, and the calculations are repeated. This procedure is continued until the transient startup analysis of the nozzle is completed. The NAC is set up to accept time periods of equal length and, for the B-1 test runs analyzed, a time period of 0.1 second was used.

The analytical equations and assumptions used in the calculation of heat-transfer rates and pressure drops in the flow stages of the single-tube model are described and discussed in appendix C.

Heat-Transfer Correlations

Heat transfer inside coolant tubes. - The correlations used to determine heat-transfer coefficients for gaseous, two-phase, and liquid-hydrogen flow inside the coolant tubes are described below:

Gaseous hydrogen flow: With gaseous hydrogen flow, the heat-transfer coefficients in equations (C4), (C9), and (C11) were determined from the conventional correlation of reference 6; that is,

$$Nu_f = 0.023\,(Re_f)^{0.8}(Pr_f)^{0.4} \tag{2}$$

The correlation presented in reference 6 was obtained from tests with gaseous

hydrogen flow at pressures from 40 to 100 pounds per square inch absolute in a circular tube with a length of 40 diameters; the wall-to-bulk temperature ratios ranged from 1.17 to 2.50. Equation (2) is strictly applicable only to the portion of the nozzle tubes where the radius of curvature is large. For the flow conditions encountered in the nozzle tubes during startup, however, the correction factor for curvature, as recommended in reference 7, was estimated to be relatively small and was therefore not included in equation (2).

The correction factor for surface roughness, as given in reference 8, was likewise determined to be small and was also neglected.

The fluid properties used in equation (2) are evaluated at the film temperature; the film temperature T_f is defined as

$$T_f = \frac{T_w + T_b}{2} \tag{3}$$

Two-phase and liquid-hydrogen flow: Although the literature pertaining to the boiling of common liquids (e.g., water, petroleum oils, etc.) is rather extensive, the data available for forced convective boiling of hydrogen are extremely limited. The little information available on boiling heat transfer for hydrogen indicates that liquid or two-phase hydrogen, because of its rather unusual properties, may be unique and that the standard techniques used in the correlation of boiling data of the common liquid may not be applicable to hydrogen.

The rate at which heat is transferred to a boiling liquid depends primarily on the heat-transfer mechanism. In the analysis presented herein, the mechanism of convective heat transfer to the two-phase and/or liquid hydrogen in the nozzle coolant tubes was assumed to be dependent only on the local calculated values of wall-to-bulk temperature differences.

Three different regimes of heat transfer were considered. The following table shows the three regimes along with the associated heat-transfer mechanisms and the ranges of wall-to-bulk temperature differences for which the mechanisms were assumed to apply.

Regime	Mechanism of heat transfer	Range of application
I	Stable nucleate boiling	$(T_w - T_b) < 4.4^\circ$ R
II	Unstable film boiling (transition boiling)	4.4° R $\leq (T_w - T_b) \leq 30^\circ$ R
III	Stable film boiling	$(T_w - T_b) > 30^\circ$ R

The ranges of wall-to-bulk temperature difference associated with the three heat-transfer mechanisms were determined from a study of the data presented in references 9 and 10.

The data in reference 9 were obtained from forced convection boiling tests conducted with hydrogen at pressures from 25 to 48 pounds per square inch absolute in an electrically heated tube with a length of 6 inches. Bulk Reynolds numbers investigated and reported in reference 9 ranged from 2×10^5 to 6.5×10^5. The maximum temperature differences between the tube wall and the boiling hydrogen for stable nucleate boiling was found to range from 3° to 6° R, depending on the pressure. The lowest temperature difference for stable film boiling was approximately 40° R. The test data presented in reference 9 were not correlated.

In reference 10, experimental pool-boiling data for liquid hydrogen are presented for pressures ranging from 42 to 266 pounds per square inch absolute. The transition from film boiling to nucleate boiling at moderate pressures was interpreted from reference 10 to occur at a wall-to-bulk temperature difference of approximately 30° R. The onset of nucleate boiling (when approached from the film-boiling regime) was estimated from reference 10 to occur at a temperature difference of approximately 4.4° R.

For the lack of more quantitative data on the wall-to-bulk temperature differences associated with the three regimes of convective boiling of hydrogen, the values of 30° and 4.4° R were used in the NAC analysis as the maximum and minimum temperature differences associated with the unstable film-boiling regime. The following heat-transfer correlations were used for the three regimes.

(1) Regime I, stable nucleate boiling - For calculated wall-to-bulk temperature differences less than 4.4° R, a nucleate-boiling mechanism of heat transfer was assumed. Reliable heat-transfer correlations for forced convection nucleate boiling of hydrogen appear to be completely lacking in the literature. Consequently, the hydrogen pool-boiling data presented in reference 10 were used to develop an approximate correlation for this regime. The equation obtained from the experimental data in reference 10 is

$$h = 0.0516\,(T_w - T_b)^2 \qquad \text{for } (T_w - T_b) < 4.4^\circ \text{ R} \tag{4}$$

(2) Regime II, unstable film boiling - For wall-to-bulk temperature differences ranging from 4.4° to 30° R, an unstable film-boiling mechanism of convective heat transfer was assumed. An approximate correlation for this regime was derived from the data in reference 10 based on the assumption that the heat flux is constant throughout the transition regime. From the data in reference 10, a constant heat flux value of 4.61 Btu per second per square foot was chosen, which corresponds to a wall-to-bulk temperature difference of 4.4° R on the nucleate-boiling curves. The heat-transfer correlation used for the unstable film-boiling regime (assuming a constant heat-flux

value of 4.61 Btu/(sec)(ft^2)) is given by

$$h = \frac{4.61}{T_w - T_b} \qquad \text{for } 4.4^\circ R \leq (T_w - T_b) \leq 30^\circ R \tag{5}$$

It should be recognized that equation (5) was developed for the purpose of bridging the gap between the stable nucleate-boiling regime and the stable film-boiling regime. For obvious reasons, steady-state heat-transfer data are not available for this regime.

(3) Regime III, stable film boiling - For wall-to-bulk temperature differences greater than 30° R, a stable film-boiling mechanism of heat transfer was assumed. Heat-transfer coefficients used in the stable film-boiling regime were computed from the following equation (ref. 11):

$$h = \frac{k_f}{D} Nu_{exp} \tag{6}$$

The experimental Nusselt number Nu_{exp} in equation (6) is expressed as a function of the Martinelli parameter $\chi_{tt,f}$ and the calculated Nusselt number Nu_{cal} as follows:

$$Nu_{exp} = \frac{Nu_{cal}}{0.706 + 1.6\,\chi_{tt,f} - 0.123(\chi_{tt,f})^2} \tag{7}$$

The Martinelli parameter $\chi_{tt,f}$ is defined by the relation

$$\chi_{tt,f} = \left(\frac{\rho_f}{\rho_{sl}}\right)^{0.5} \left(\frac{\mu_{sl}}{\mu_f}\right)^{0.1} \left(\frac{1 - X}{X}\right)^{0.9} \tag{8}$$

The subscript f on the Martinelli parameter indicates that the gas-phase properties are evaluated at the film temperature. The calculated Nusselt number is computed from the relations given in reference 11.

Heat transfer from hot side of nozzle. - Many correlations have been presented in the literature for the evaluation of heat-transfer coefficients for the hot gas side of nozzles. A comparison of the available correlations revealed that the computed values of local hot-gas-side heat-transfer coefficients may differ considerably, depending on the particular correlation used.

The hot-gas-side heat-transfer coefficients used in equations (C1) and (C6) were computed from a modified pipe-flow heat-transfer correlation similar to that presented

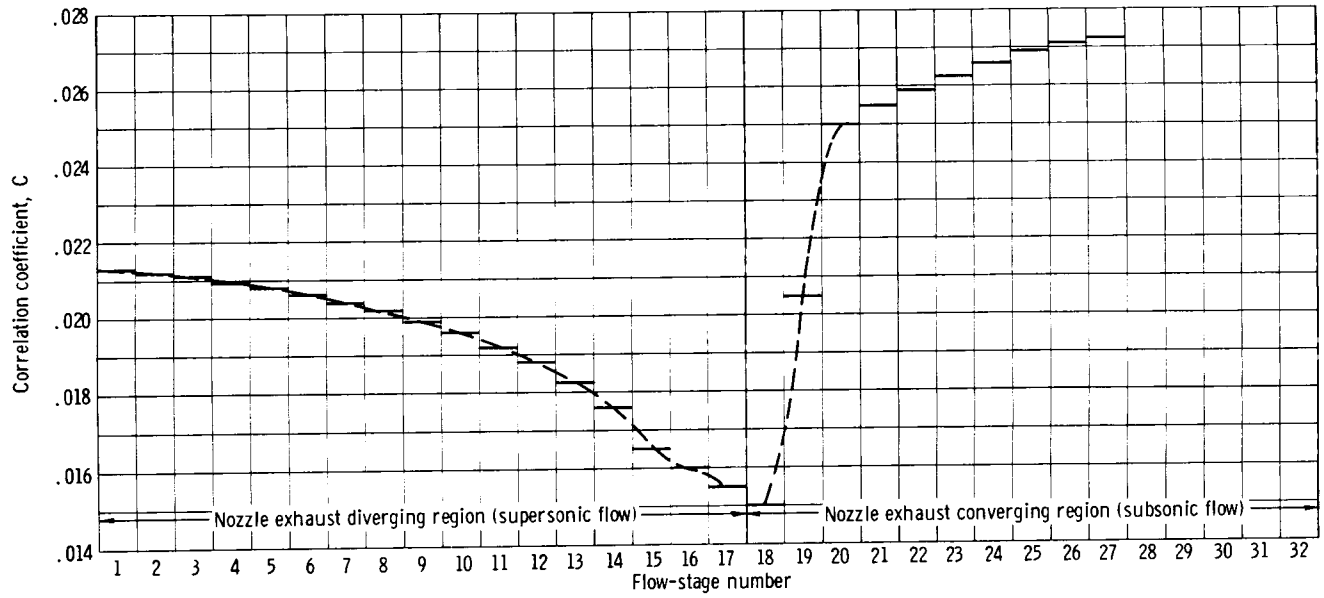

Figure 9. - RN-2 nozzle exhaust side heat-transfer correlation coefficient as function of flow-stage number.

in reference 12. This correlation uses a variable coefficient C, which is an experimentally determined value expressed as a function of the nozzle-area ratio. The modified Nusselt equation used in the NAC to evaluate the local coefficients on the hot gas side of the nozzle is

$$Nu_{fm} = C(Re_{fm})^{0.8}(Pr_{fm})^{0.4} \tag{9}$$

The values of C used for the flow stages of the RN-2 nozzle are shown in figure 9; these coefficients were taken from the experimental data in reference 12. The coefficients presented in reference 12 were obtained from transient heat-transfer tests conducted with a conical nozzle that had a 5-inch-diameter throat and a 4.64 expansion and contraction ratio.

Since the expansion and contraction area ratios for the RN-2 nozzle were larger than 4.64, some of the values plotted in figure 9 were estimated from an extrapolation of the data in reference 12.

The local fluid properties used in equation (9) were evaluated and based on a static pressure and a partial recovery film temperature. The local static pressure was computed from the following relation (ref. 13):

$$\mathscr{P}_s = \frac{\mathscr{P}_t}{\left(1 + \frac{\gamma - 1}{2} M^2\right)^{\gamma/\gamma-1}} \tag{10}$$

The partial recovery film temperature T_{fm} was calculated from

$$T_{fm} = \frac{T_w + T_{cm}}{2} \tag{11}$$

The temperature T_{cm} in equation (11) represents a nine-tenths fluid recovery temperature and is defined as

$$T_{cm} = T_{ct} - 0.10\, T_{cs} \frac{\gamma - 1}{2} M^2 \tag{12}$$

where T_{ct} and T_{cs} are the local total and static fluid temperatures, respectively. The nine-tenths fluid recovery temperature T_{cm} is also used in the calculation of forced convection heat-transfer rates on the hot gas side of the nozzle (see appendix C, eqs. (C1) and (C6)). As suggested in reference 14, for gas flow at high velocity, the

value of the fluid bulk temperature used in calculation of heat-transfer rates should be based on a reference enthalpy condition. The nine-tenths fluid recovery temperature T_{cm} used in equations (C1) and (C6) is a close approximation of the reference temperature suggested in reference 14.

The surface area for heat transfer from the hot gas side of the RN-2 nozzle $A_{s,hs}$ was determined by assuming that the inner nozzle surface was smooth. (The inner surface of the RN-2 nozzle has a scalloped or corrugated appearance because of the tubular wall construction.) Since the RN-2 nozzle is made up of 180 coolant tubes, the surface areas for the individual flow stages of the single-tube model were computed as 1/180 of the product of the flow-stage length and the appropriate total nozzle (smooth) perimeter.

Friction Factor Relations

Gas flow. - For turbulent gas flow inside the coolant tubes, the friction factors for the individual flow stages were computed from the following relation:

$$f_j = C_a(0.046)(Re_{j,b})^{-0.20} \tag{13}$$

The coefficient C_a in equation (13) is a correction factor to account for tube curvature and is defined in reference 7 as

$$C_a = \left[Re_{j,b}\left(\frac{R}{r}\right)^2\right]^{0.05} \tag{14}$$

As suggested in reference 7, the coefficient C_a should be used for $R/r \geq 6$. For $R/r < 6$, $C_a = 1.0$, and equation (13) is equivalent to the Blasius equation (ref. 15). The local bulk Reynolds number used in equations (13) and (14) is given by

$$Re_{j,b} = \left(\frac{\dot{\omega}_c D_j}{A_j \mu_j}\right)_b \tag{15}$$

The local friction factors for turbulent gas flow computed from equation (13) were used in equation (C18) to compute the friction pressure losses in the individual flow stages. (For the B-1 test runs, the flow in the nozzle coolant tubes is turbulent throughout a transient chilldown; therefore, a laminar-flow friction factor correlation was not required.)

The curvature correction factor as calculated by equation (14) was relatively small for the range of bulk Reynolds numbers encountered in the startup transient.

Two-phase flow. - The friction factors for two-phase turbulent flow were computed from a modified form of equation (13) in which a gas-phase Reynolds number was used. The gas-phase Reynolds number (ref. 16) is given by

$$Re_{j,sg} = \frac{X_j \dot{\omega}_c D_j}{A_j \mu_{j,sg}} \tag{16}$$

The friction factors used in equation (C20) to compute the gas-phase friction pressure losses in the individual flow stages were obtained from the following relation:

$$f_j = C_a(0.046)(Re_{j,sg})^{-0.20} \tag{17}$$

The coefficient C_a for two-phase turbulent flow is given by

$$C_a = \left[Re_{j,sg}\left(\frac{R}{r}\right)^2\right]^{0.05} \tag{18}$$

Subcooled liquid flow. - The friction factors for turbulent flow of subcooled liquid hydrogen were computed from equation (13). The Reynolds numbers in the friction factor relation were evaluated from equation (15) and were based on the local bulk properties of the subcooled liquid phase.

RESULTS AND DISCUSSION

The terms in each of the three groups of input data for the NAC are defined in appendix B. As stated previously, the time-dependent input conditions for the NAC are obtained (directly or indirectly) from experimental measurements.

The time-dependent input conditions used in the NAC for liquid-hydrogen test run 24 are shown in figures 10 to 13. The hydrogen temperature, pressure, and quality at the inlet to the nozzle coolant tubes are shown as a function of time in figure 10. The single-passage flow rate is shown as a function of time in figure 11. Figure 12 shows the hydrogen temperature and pressure as a function of time at the nozzle chamber inlet, and figure 13 shows the total flow rate on the hot gas side of the nozzle as a function of time. The sources from which these input data (figs. 10 to 13) were obtained are indicated on the respective figures.

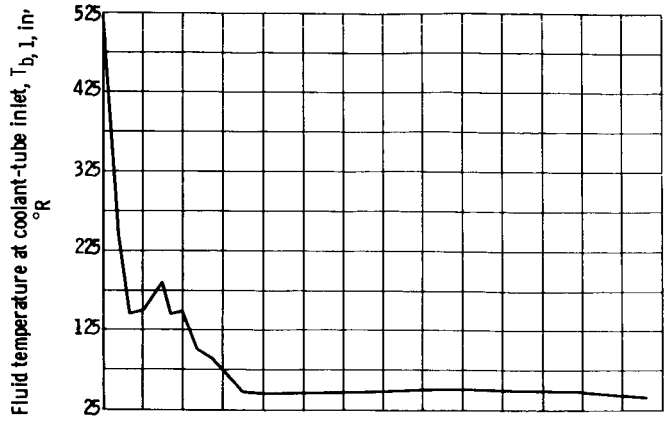

(a) Fluid temperature conditions (data from average of items NR-1, NR-2, and NR-4).

(b) Static pressure conditions (data from item NP-1).

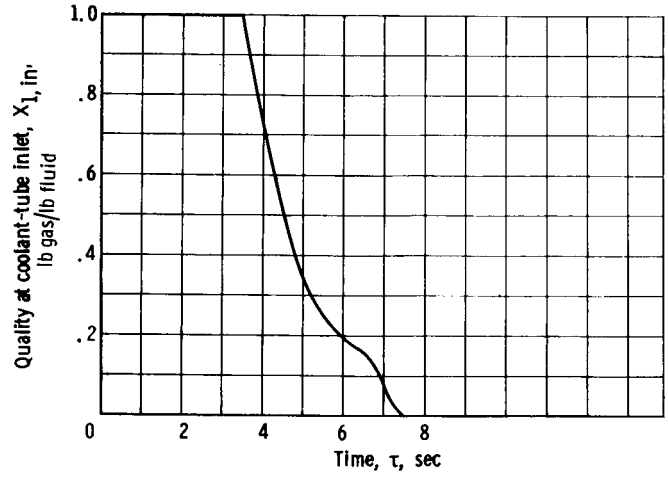

(c) Fluid quality conditions (data from ref. 3).

Figure 10. - Conditions at coolant-tube inlet as functions of time for liquid-hydrogen test run 24.

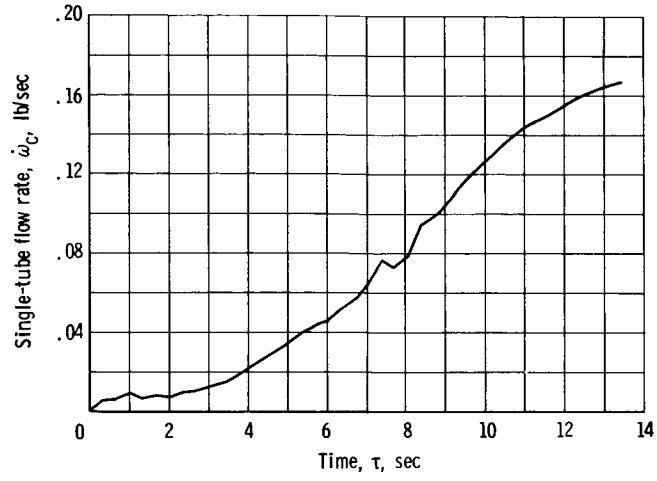

Figure 11. - Flow rate of single RN-2 nozzle coolant tube as function of time for liquid-hydrogen test run 24 (data from ref. 3).

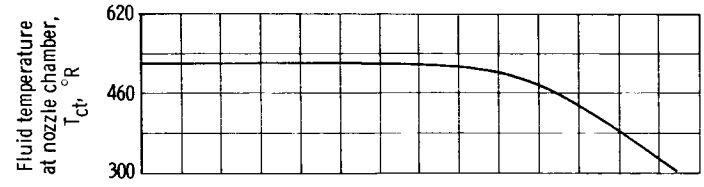

(a) Fluid temperature conditions (data from average of items NT-60, NT-61, NT-62, NT-63, and NT-64).

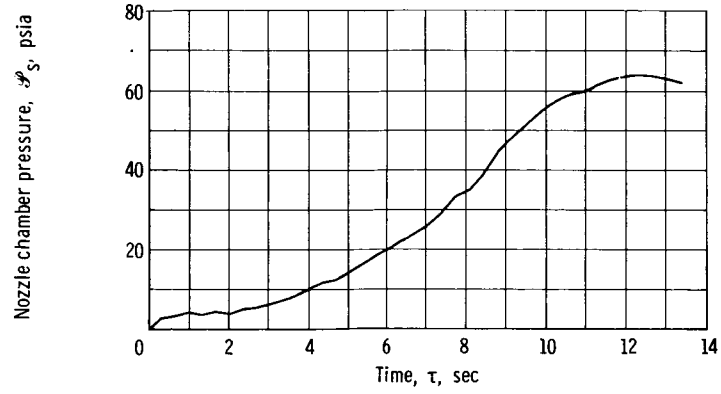

(b) Pressure conditions (data from item NP-50).

Figure 12. - Conditions at nozzle chamber inlet as functions of time for liquid-hydrogen test run 24.

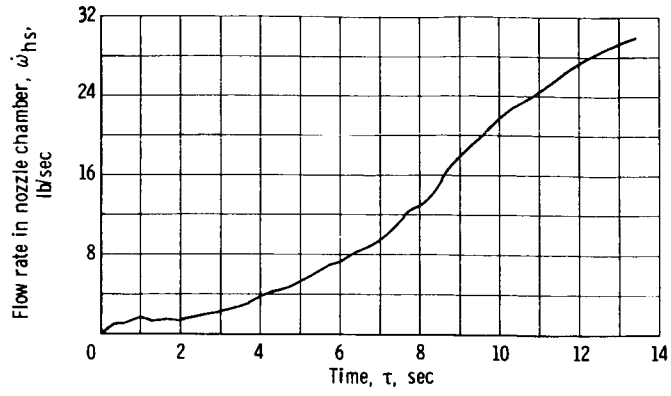

Figure 13. - Total flow rate in RN-2 nozzle chamber as function of time for liquid-hydrogen test run 24 (data from ref. 3).

The important parameters for liquid-hydrogen test run 24 are as follows:

Propellant storage tank pressure, psia	35
Approximate total run time, sec	13.5
Approximate flow rate range, lb/sec	0 to 30
Approximate nozzle inlet manifold pressure range, psia	1 to 130
Temperature of nozzle assembly at time zero, ^{o}R	510

The locations of the nozzle instrumentation for liquid-hydrogen test run 24 are shown in figure 4 (p. 8). As pointed out, most of the nozzle measurements for run 24 were concentrated on 3 of the 180 coolant tubes.

In the following section, the experimental data obtained from measurement locations shown in figure 4 are presented and compared with values calculated from the NAC.

Comparison of Calculated and Measured Data

Coolant-tube temperatures. - The experimental and calculated coolant-tube temperatures at various positions along the length of the nozzle are presented as a function of time in figure 14. The calculated temperatures from the NAC are identified in this figure with solid lines, and the experimental measurements are identified with symbols. The state of the hydrogen entering the nozzle coolant tubes during the test run is also indicated. For times less than 3.5 seconds, the hydrogen flow in the nozzle tubes was gaseous. From 3.5 to 7.5 seconds, the flow entering the nozzle tubes was a two-phase mixture and, for times greater than 7.5 seconds, the flow entering the coolant tubes was in a subcooled liquid state.

An inspection of the data in figure 14 indicates that the time constant for the chill-

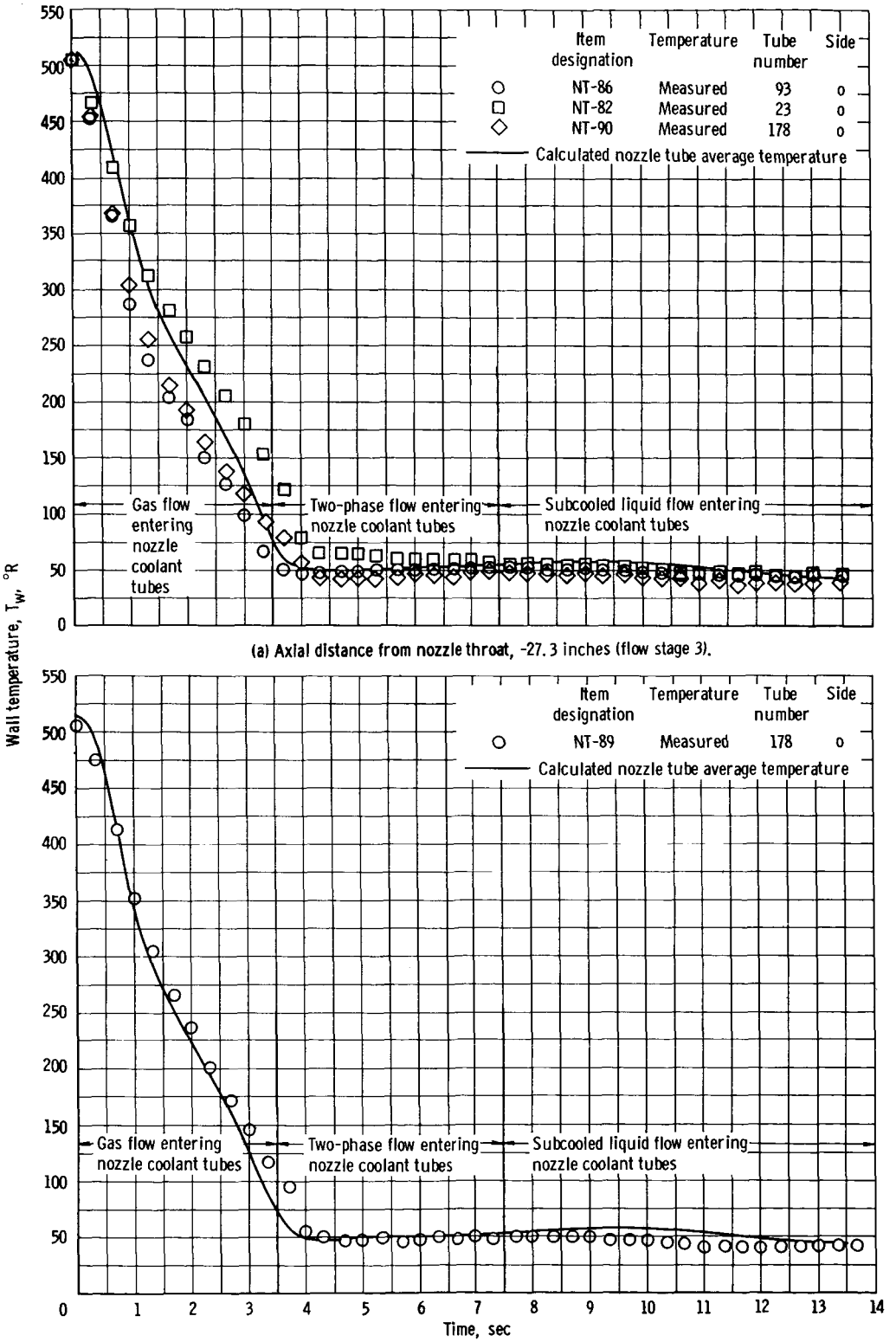

(a) Axial distance from nozzle throat, -27.3 inches (flow stage 3).

(b) Axial distance from nozzle throat, -23.3 inches (flow stage 5).

Figure 14. - Comparison of measured and calculated coolant-tube temperatures at various axial distances from nozzle throat as function of time for liquid-hydrogen test run 24.

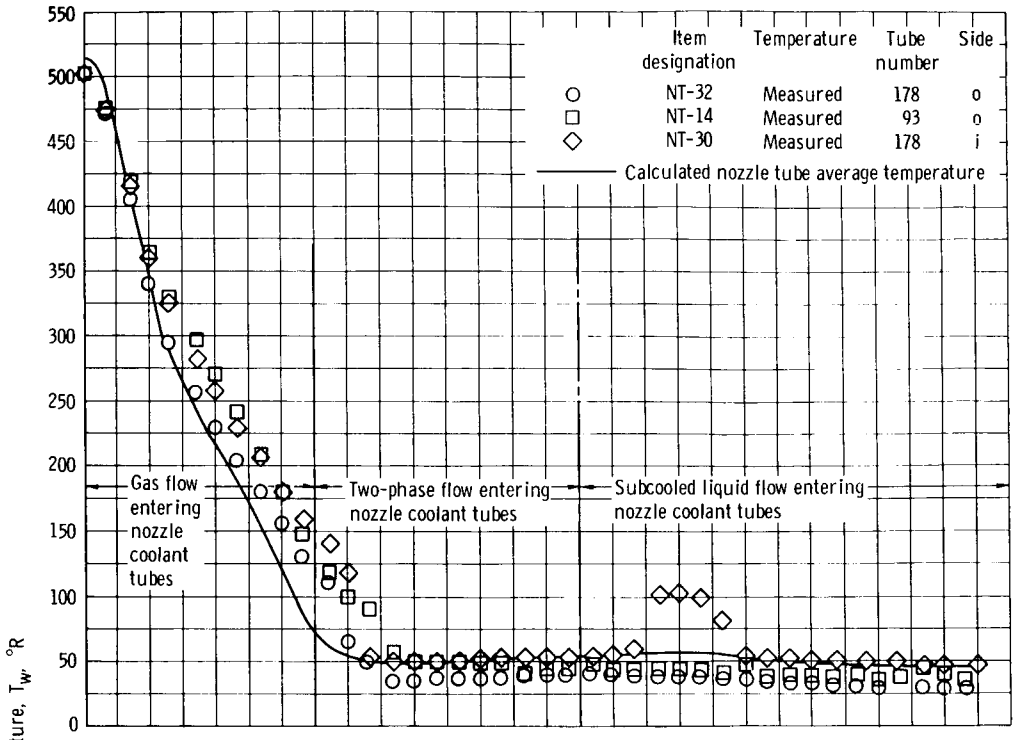

(c) Axial distance from nozzle throat, -19.6 inches (flow stage 7).

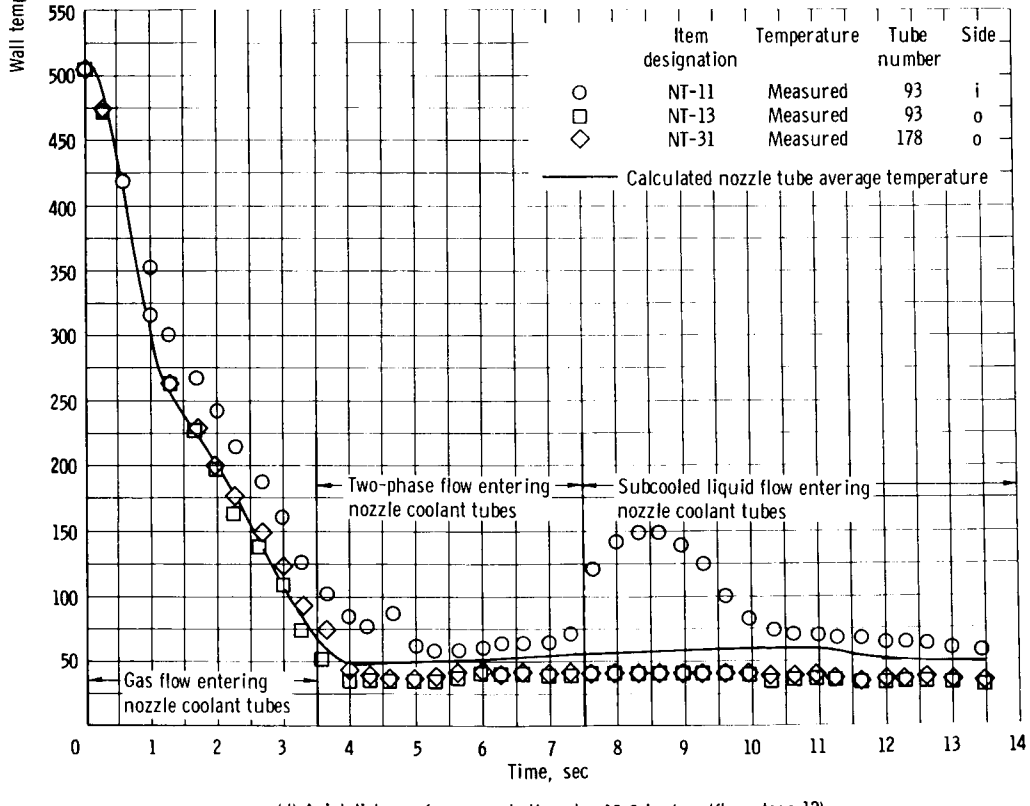

(d) Axial distance from nozzle throat, -10.3 inches (flow stage 12).

Figure 14. - Continued.

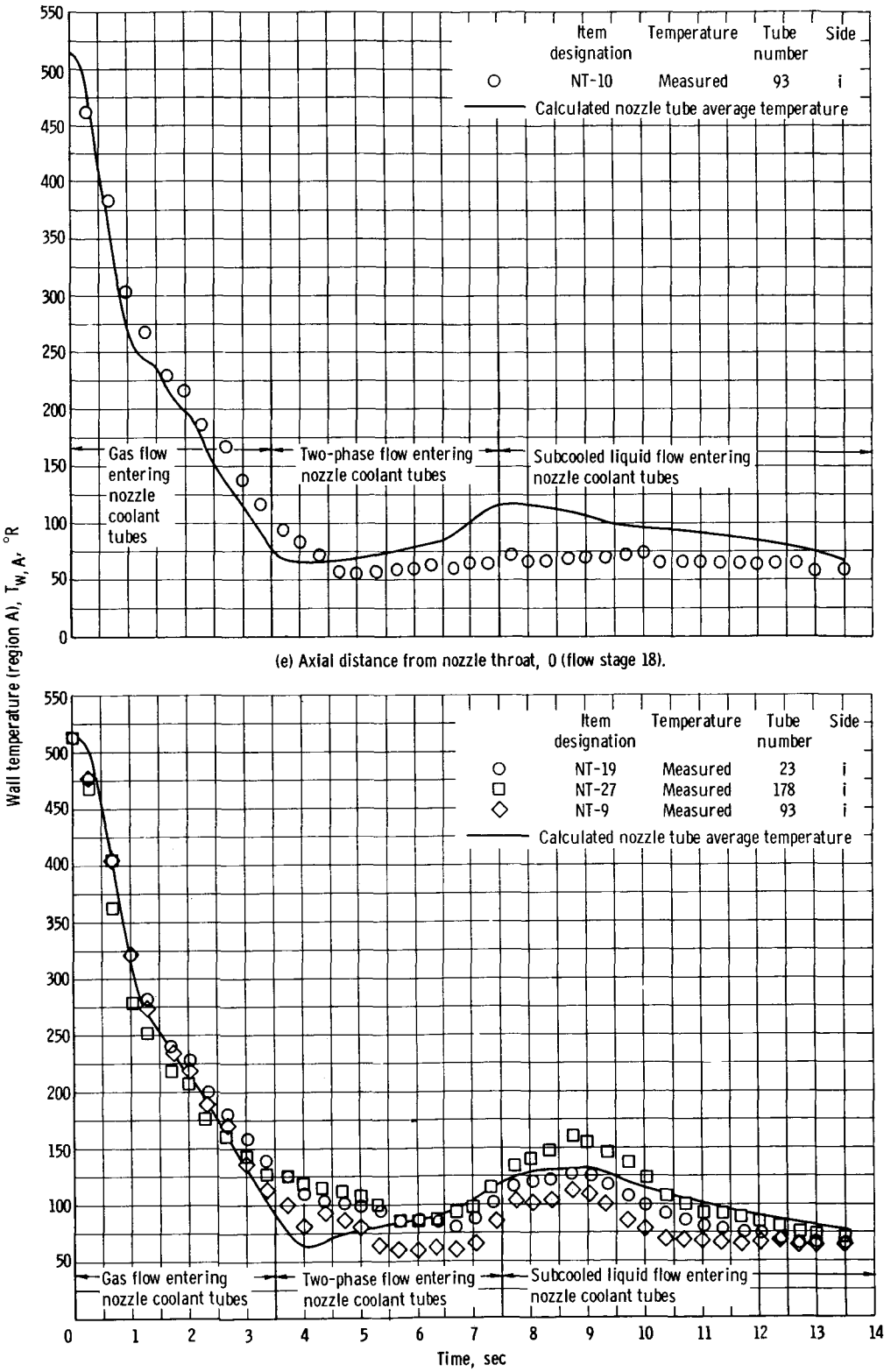

(e) Axial distance from nozzle throat, 0 (flow stage 18).

(f) Axial distance from nozzle throat, 6.6 inches (flow stage 21).

Figure 14. - Continued.

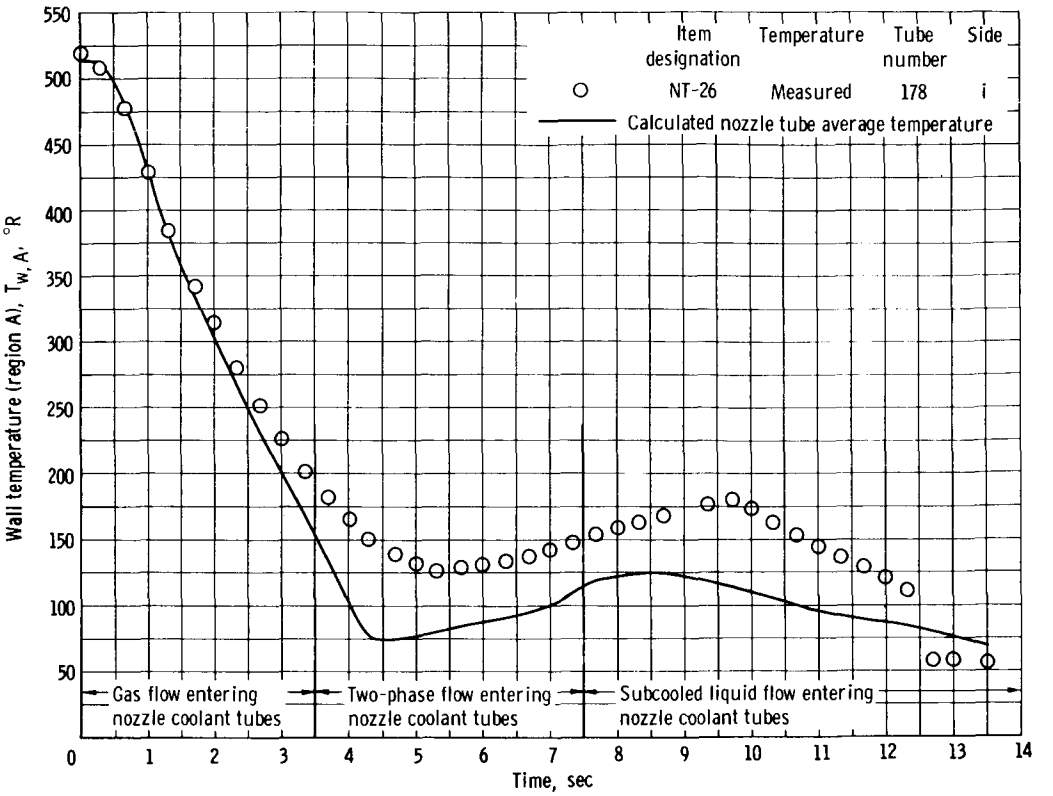

(g) Axial distance from nozzle throat, 13.2 inches (flow stage 26).

Figure 14. - Concluded.

down of the nozzle tubes is extremely small. For example, the coolant tube temperature in the vicinity of the nozzle tube inlet (figs. 14(a) to (c)) is reduced from about 510° R to approximately 50° R in the first 4 seconds of the chilldown transient.

In a comparison of the calculated and measured data in figure 14, it should be noted that the predicted temperatures represent an average value over a flow-stage length of the single-tube model, whereas the measured values are indicative of the temperature at a local point on the coolant-tube surfaces. In addition, it should be noted that the calculated coolant-tube temperatures were based on the assumption that the flow conditions are identical in each of the coolant tubes in the nozzle assembly.

An inspection of the experimental data shows that the chilldown characteristics of the three instrumented coolant tubes in the nozzle assembly are somewhat different, particularly in the early part of the test run. The differences in the measured local temperatures of these tubes, as shown in figures 14(a), (c), and (d), for example, are interpreted as a qualitative indication that the flow conditions in each of the 180 nozzle coolant tubes were not identical during the early part of the chilldown transient.

In addition to the variation in the chilldown characteristics of the different tubes, some marked nonuniformities were noted in the material temperatures measured at dif-

ferent points on the periphery of individual tubes. An indication of these local temperature differences is given by the experimental data in figures 14(c) and (d). In figure 14(d) measured coolant-tube material temperatures are shown for the inside and the outside surfaces of the nozzle at axial position x of -10.3 inches. (Inside and outside as stated herein refer to the portions of the coolant tubes that form the inside and outside surfaces of the nozzle assembly, respectively. See fig. 4 for the locations of these thermocouples.) The data in figure 14(d) show that the measured material temperatures on the inside and the outside of coolant tube 93 differ by a significant amount, particularly in the time period from 7 to 10 seconds. A similar, although less severe, temperature difference is shown in figure 14(c) for coolant tube 178. The sharp rise and decay of the inside surface temperatures shown in figures 14(c) and (d) are attributed to a transition in the local two-phase convective heat-transfer mechanism on the coolant-side surfaces of these tubes. Obviously, a local transition of this type is difficult to predict. The sudden temperature increases shown in these figures result from the fact that, with unstable film boiling on a portion of the coolant-side surfaces, the rate of heat input from the hot gas side of the nozzle becomes larger than the rate of heat removal from the coolant-side surfaces.

In a comparison of the calculated and measured temperatures in figure 14, it should be recalled that the experimental values were obtained from measurements made on only 1 or more of 3 instrumented tubes in the nozzle assembly. As such, the temperatures measured on these 3 tubes may not be representative of the average temperature of all 180 tubes in the assembly.

Nevertheless, the calculated and measured temperatures in figure 14 exhibit similar trends. From the limited experimental data obtained for test run 24, it appears that the nozzle chilldown characteristics predicted from the NAC are reasonable.

The calculated and experimental coolant-tube temperatures in figures 14(a), (b), (c), and (d) (which represent the four different axial locations on the convergent length of the nozzle tubes) are, for the most part, in good agreement. Aside from the local inflections of the temperature data in figures 14(c) and (d), the calculated coolant-tube temperatures for these four axial locations are considered to be within or reasonably near the experimental accuracy of the measured material temperatures. It should be recognized that the material temperature measurements made with copper-constantan thermocouples below about 100° R are subject to considerable error. As stated in the Instrumentation section, for the B-1 system, the errors associated with measurements made with copper-constantan in the liquid-hydrogen temperature regime may be as much as $\pm 15^{\circ}$ R.

The largest relative differences in predicted and measured local coolant-tube temperatures occurred at locations on the divergent length of the nozzle tubes, especially during the two-phase and liquid-flow portions of the test run. The calculated and measured temperatures at three positions on the divergent segment of the nozzle tubes are shown in figures 14(e) to (g).

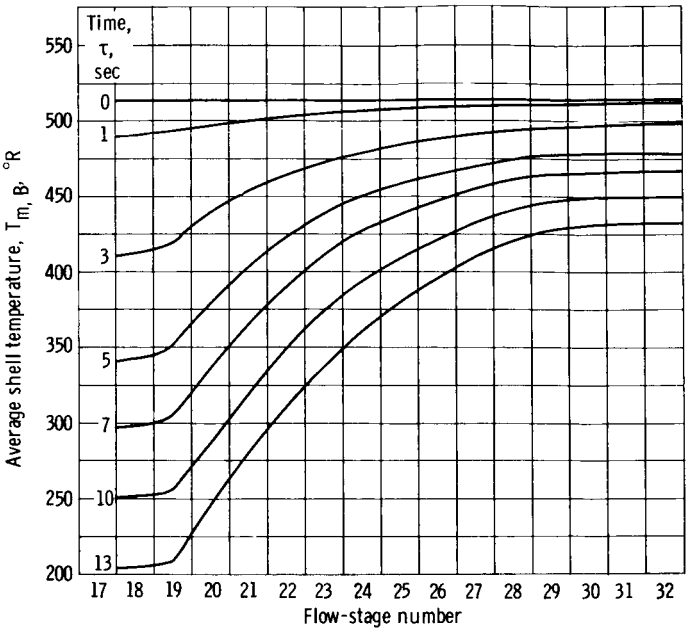

Figure 15. - Axial distribution of RN-2 nozzle-shell average temperature at various times.

A significant portion of the difference between calculated and measured temperatures in these figures is believed to be caused by differences in the predicted and actual mechanisms of local heat transfer, which takes place inside the coolant tubes. The convective heat input to the coolant tubes from the warm hydrogen gas flowing inside the nozzle assembly tends to raise the coolant-tube wall temperature which, in turn, has a significant influence on the mechanism of convective boiling heat transfer on the inside surface of the coolant tubes.

Throughout the two-phase and liquid-flow portions of the test run, the temperature difference between the coolant-tube wall and the hydrogen inside the tubes was such that an unstable mechanism of two-phase boiling could exist.

As stated in the ANALYTICAL PROCEDURE section, sufficient experimental data for forced convective boiling of hydrogen are not presently available. The assumed wall-to-bulk temperature differences used in the analysis to predict the heat-transfer mechanisms and coefficients for two-phase and liquid-hydrogen flow were estimated from limited experimental data.

It is generally felt that additional experimental and analytical study is required to obtain improved correlations for predicting two-phase hydrogen heat transfer, particularly in the regime of low wall-to-bulk temperature differences.

Nozzle support-shell temperatures. - The axial distributions of calculated average support-shell temperatures at different times during liquid-hydrogen test run 24 are shown in figure 15. The minimum value of the shell average temperature at each point in time occurs in the vicinity of the nozzle throat. From the data in figure 15, it is seen

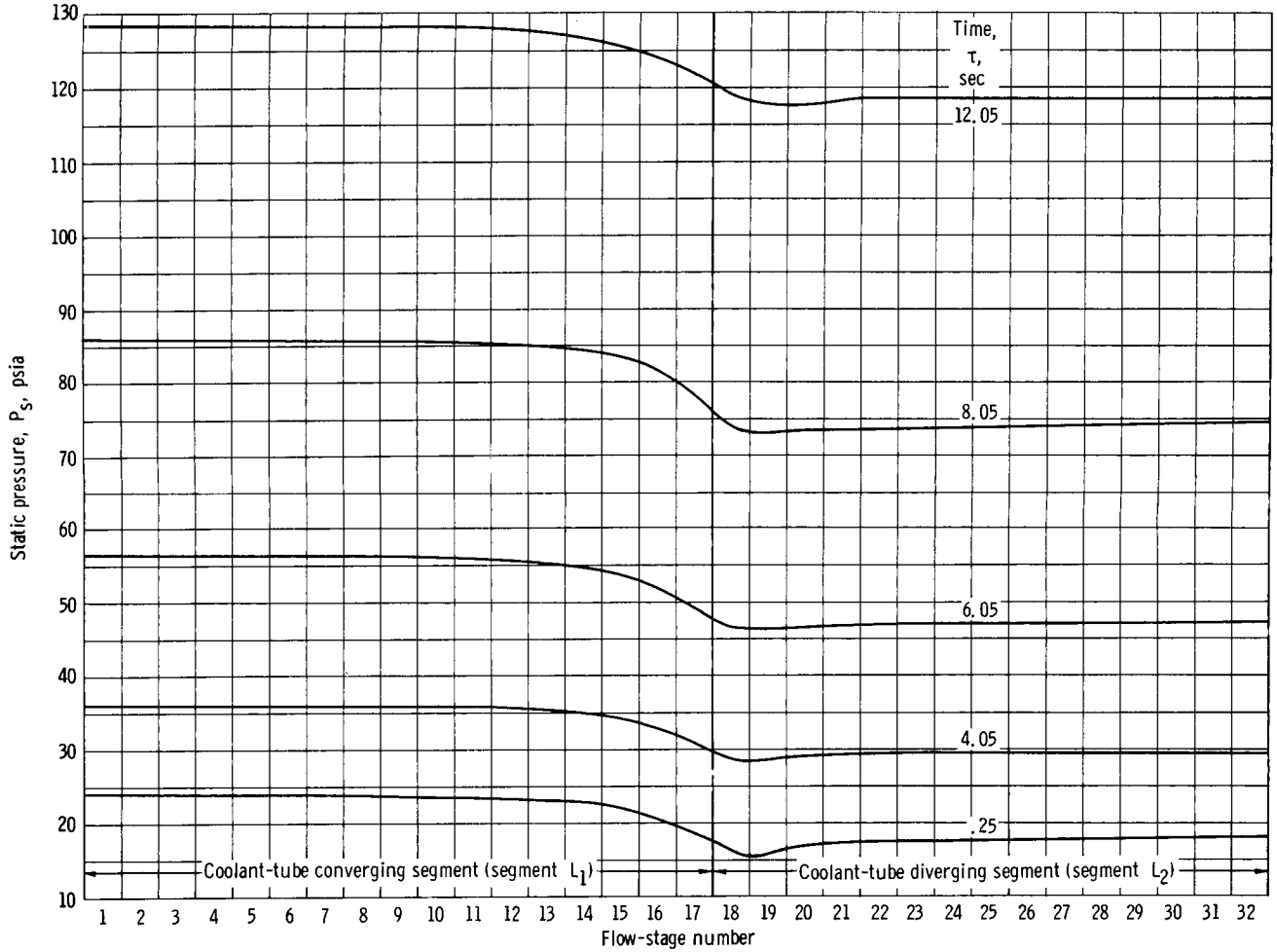

Figure 16. - Computed static pressure distributions in RN-2 nozzle coolant tubes at various times for liquid-hydrogen test run 24.

that the calculated change in temperature of the support shell with respect to time is relatively small compared with that of the nozzle coolant tubes.

As indicated in figure 4 (p. 8), temperature measurements were made at only two points on the outer surface of the support shell. Because of temperature gradients across the shell thickness, the calculated shell temperatures in figure 15 (which are average local values) could not be compared directly with the local measured surface temperatures.

Coolant-tube pressure data. - Figure 16 shows the calculated static pressure distributions in the nozzle coolant tubes at several different points in time. An inspection of these data shows that the minimum static pressure along the tube length occurs at a point somewhat downstream of the coolant-tube throat. This is explained by the fact that the calculated friction and momentum pressure drops in the two flow stages downstream of the throat, that is, stages 18 and 19, are, for the most part, larger than the pressure recoveries due to expansion.

The data in figure 16 show that the calculated static pressure loss across flow stages 15 to 19 accounts for approximately 90 percent of the overall static pressure loss in the nozzle coolant tubes. An interesting feature of the pressure distributions shown in figure 16 is that the calculated static pressures at the nozzle coolant-tube throat (stage 18 inlet) are nearly equal to the static pressures at the coolant-tube outlet (stage 32).

Figure 17 shows a comparison of calculated and measured static pressures at the coolant-tube outlet. The measured static pressures at the inlet to the nozzle coolant tubes are also shown in figure 17. In the time ranges of 0 to 7.5 seconds and 10.5 to 13 seconds, the calculated and experimental pressures at the coolant-tube outlet show reasonable agreement; for the most part, the predicted pressures are within the experimental accuracy of the measured values. (The estimated accuracy of the measured pressures shown in fig. 17 was given in the Instrumentation section as ±2 psi.)

For the time span from approximately 7.5 to 10.5 seconds, the experimental and calculated pressures at the coolant-tube outlet differ by significant amounts. As shown in figure 17, the calculated pressure drops in this time span are approximately twice as large as the measured pressure differences.

The estimated state of the hydrogen in the nozzle coolant tubes for different time spans of the test run is indicated in the following table:

Time span, sec	Hydrogen state
0 to 3.5	Superheated gas flow throughout nozzle tubes
3.5 to 4.8	Two-phase flow entering and superheated gas flow leaving coolant tubes
4.8 to 7.5	Two-phase flow throughout nozzle tubes
7.5 to 11.5	Subcooled liquid flow entering and two-phase flow leaving coolant tubes
11.5 to 13.5	Subcooled liquid flow throughout nozzle tubes

For times greater than 7.5 seconds, the hydrogen entering the nozzle coolant tubes was subcooled. However, the computed heat input to the hydrogen in the time period from 7.5 seconds to about 10.2 seconds resulted in a transition from a subcooled liquid state to a two-phase state at some point in the tubes between the tube inlet and tube throat. As a result, the major portion of the calculated pressure loss occurred in the length of the tubes that had two-phase flow. (It should be remembered that the major portion of the overall static pressure loss in the tubes takes place in flow stages 15 to 19.)

Of significance also is that, in the later part of the test run, that is, for times greater than about 6 seconds, the change in fluid bulk density along the length of the nozzle tubes was small and, as a consequence, the calculated static pressure loss in the tubes was primarily caused by friction.

The fact that the predicted pressure drops are considerably higher than the measured values from 7.5 to 10.5 seconds might be explained on the basis that the Martinelli two-phase pressure-drop relations (which were used in this analysis and are described in appendix C) overestimate the frictional pressure drops of two-phase hydrogen flow, particularly when the fluid quality is near zero.

Unfortunately, there are no published experimental correlations for predicting two-phase frictional pressure drops for forced convective boiling of hydrogen. Many factors may effect the frictional pressure loss, such as relative velocity between gas and liquid phases, the size and distribution of liquid droplets, and the intensity of turbulence in the flow mixture. The change in these variables with position along a heated flow passage is difficult to express analytically.

A limited experimental investigation of two-phase pressure drop with hydrogen is reported in reference 17; the data from these experiments, however, were not correlated.

When the experimental pressure-drop data presented in reference 17 were compared with pressure drops predicted by the Martinelli relations, it was found that the Martinelli relations gave predicted pressure drops which, for the most part, were

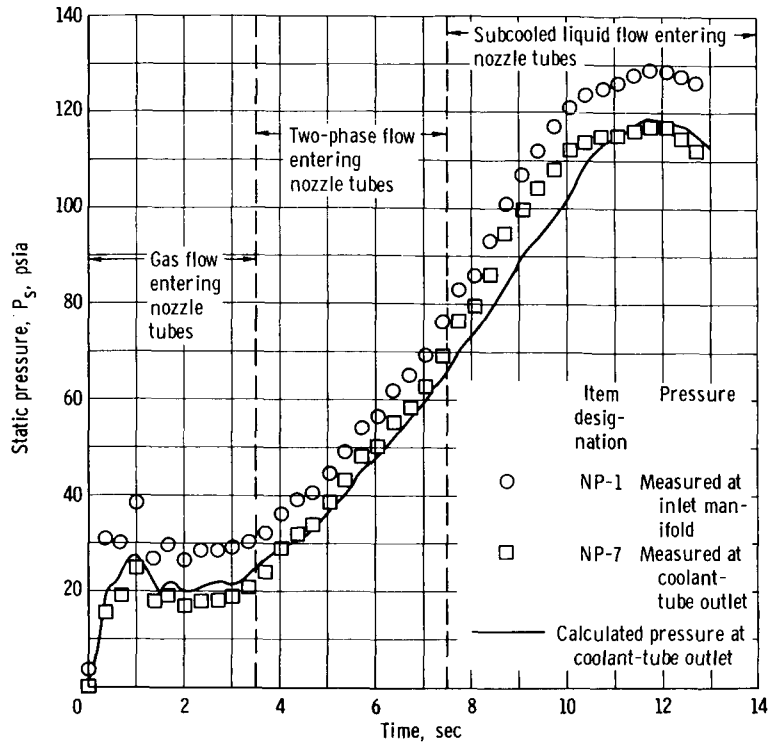

Figure 17. - Comparison of measured and computed static pressure at RN-2 nozzle coolant-tube outlet as function of time for liquid-hydrogen test run 24.

significantly larger than the experimental values, especially in the region of low fluid quality.

Inasmuch as the data presented in reference 17 were somewhat limited and were not correlated, it appears that additional study is needed before a satisfactory method can be achieved for calculating the frictional pressure drops for forced convective boiling of two-phase hydrogen.

Hydrogen quality distribution. - The calculated hydrogen quality distributions in the RN-2 nozzle coolant tubes are shown for various times of liquid-hydrogen test run 24 in figure 18. An inspection of the curves shows that the predicted change in quality along the length of the nozzle tubes is large in the early part of the run and becomes smaller with time as the inlet quality decreases.

For times greater than about 5 seconds, the increases in hydrogen quality along the length of the nozzle tubes resulted primarily from heat additions from the nozzle support shell and the countercurrent flow of warm hydrogen gas in the nozzle exhaust. (Data in fig. 14 show that nearly all the sensible heat of the nozzle coolant tubes is removed in the first 5 seconds of the test run.) Of significance is the fact that the calculations indicate that, in the later portion of the test run, approximately 80 percent of the combined heat input to the two-phase and liquid hydrogen was caused by the convective heat trans-

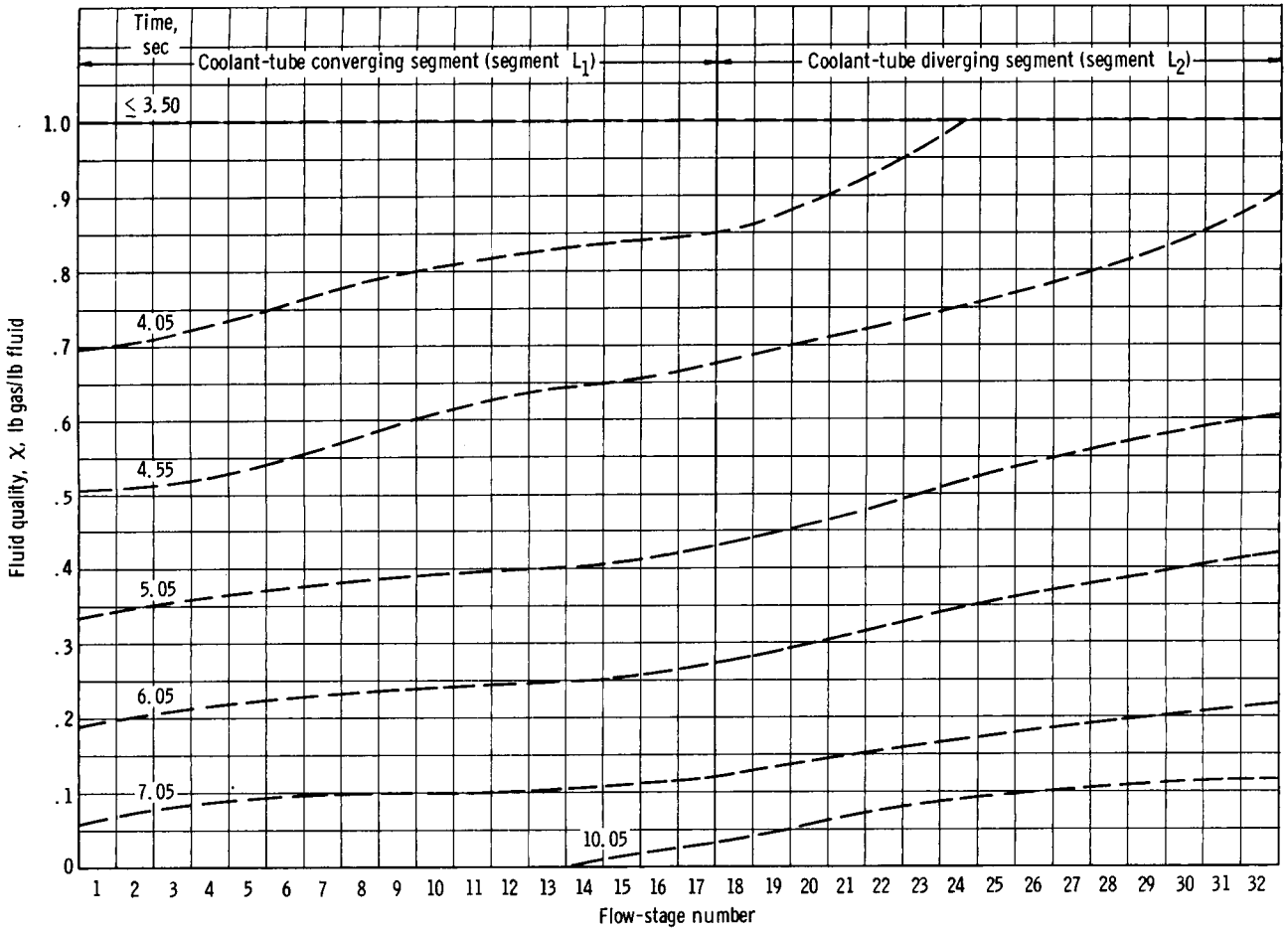

Figure 18. - Computed para-hydrogen quality distributions in RN-2 nozzle coolant tubes at various times for liquid-hydrogen test run 24.

fer from the warm hydrogen gas in the nozzle exhaust.

SUMMARY OF RESULTS

The analytical and experimental investigations of the startup characteristics of the regeneratively cooled nozzle used in the cold-flow nuclear rocket test system yielded the following principal findings:

1. The time constant for the chilldown of the nozzle coolant tubes is extremely small. For the test run reported herein, the coolant-tube temperatures near the nozzle tube inlet were reduced from about 510° R to approximately 50° R in the first 4 seconds of the startup transient.

2. The measured chilldown characteristics of three instrumented coolant tubes in the nozzle assembly were found to be somewhat different, particularly in the early part of the test run. In addition to the variation in chilldown characteristics of different tubes in the nozzle assembly, some marked nonuniformities were noted in local material temperatures measured on the inside and outside of individual tubes at the same axial locations. These nonuniformities were attributed to a transition in the local forced convective boiling heat-transfer mechanism on the coolant-side surfaces of these tubes.

3. In general, the calculated and measured temperatures of the nozzle coolant tubes exhibited similar trends. Aside from local inflections in the measured temperatures (caused by transitions in the two-phase boiling mechanisms), the calculated material temperatures for the convergent segment of the nozzle tubes were considered to be within or reasonably near the experimental accuracy of the measured material temperatures. The largest relative differences in predicted and measured local coolant-tube temperatures occurred at locations on the divergent length of the nozzle tubes during the two-phase and liquid flow portions of the test run. A significant part of the disagreement in predicted and measured temperatures is believed to be caused by differences in the predicted and actual mechanisms of local convective boiling inside the coolant tubes.

4. Throughout most of the test run, the calculated and measured static pressure drops in the nozzle tubes showed reasonable agreement. However, during the time period in which the two-phase hydrogen flow mixture was predominately liquid, the calculated pressure drops were considerably larger than the measured values. A possible explanation of this difference (based on limited published data for two-phase frictional pressure drops with hydrogen) is that the Martinelli relations, which were used in the pressure-drop analysis, have a tendency to overestimate the frictional loss for

two-phase hydrogen flow, particularly when the quality of the two-phase flow mixture approaches zero.

Lewis Research Center,
National Aeronautics and Space Administration,
Cleveland, Ohio, October 21, 1966,
122-29-01-07-22.

APPENDIX A

SYMBOLS

A	flow area, ft^2
A_s	surface area for heat transfer, ft^2
C	correlation coefficient in eq. (9) and fig. 9
C_a	correlation factor to account for tube curvature (eq. (14))
c_m	specific heat of nozzle material, Btu/(lb)(^oR)
c_p	specific heat of hydrogen at constant pressure, Btu/(lb)(^oR)
D	hydraulic diameter of flow stage, ft
d	nozzle exhaust side hydraulic diameter, ft
f	Fanning friction factor
g	conversion factor, 32.174 ft/sec^2
h	convective heat-transfer coefficient, Btu/(sec)(ft^2)(^oR)
i	portion of tube surface that is contacted by gas in nozzle chamber
k	thermal conductivity of hydrogen gas, Btu/(sec)(ft)(^oR)
L_1	segment of RN-2 nozzle extending from nozzle inlet manifold to nozzle throat, ft
L_2	segment of RN-2 nozzle extending from nozzle throat to coolant-tube outlet, ft
l	flow-stage length, ft
M	Mach number
Nu	Nusselt number
Nu_{cal}	Nusselt number calculated from modified Dittus-Boelter equation
Nu_{exp}	experimental Nusselt number for two-phase flow (eq. (7))
o	portion of tube surface that is furthest from chamber gas stream
P	pressure, psia
Pr	Prandtl number
$\mathscr{P}$	pressure on hot gas side of nozzle, psia
Q	heat transferred from single flow stage in time period $\tau_i - \tau_{i-1}$, Btu per time period
q	heat transferred from hot gas side of nozzle to coolant-tube wall in time period $\tau_i - \tau_{i-1}$, Btu per time period
R	radius of coolant tube, D/2, ft
Re	Reynolds number
R_g	specific gas law constant for hydrogen, 766 ft/^oR
$\mathscr{R}$	radial distance from nozzle axis, in.
r	radius of curvature of nozzle tubes, ft
T	temperature, ^oR
v	average fluid velocity inside of coolant tubes, ft/sec

W_m	weight of material assigned to flow stage or flow-stage region, lb
X	fluid quality, lb_{gas}/lb_{fluid}
x	axial distance from nozzle throat, in.
γ	ratio of specific heats, c_p/c_v
θ	reference angle
λ	heat of vaporization, Btu/lb
μ	viscosity, lb/(ft)(sec)
ρ	fluid density, based on local static temperature and pressure, lb/ft^3
T	total time span of test run, sec
τ	time, sec
Φ_{tt}	coefficient in pressure-drop equation (eq. (C19))
χ_{tt}	Martinelli two-phase parameter (both phases turbulent) (eq. (8))
$\dot{\omega}$	mass flow rate, lb/sec

Subscripts:

A	region A
av	average
B	region B
b	bulk
c	coolant flow rate in single nozzle coolant tube (eq. (1))
cm	nine-tenths fluid recovery temperature (eq. (12))
cs	static fluid temperature on hot gas side of nozzle (eq. (12))
ct	total fluid temperature on hot gas side of nozzle (eq. (12))
f	film
fluid	gas and liquid phases
fm	partial recovery film temperature for hot gas side of nozzle (eq. (11))
fr	friction
gas	weight fraction of two-phase fluid that is gas
hs	hot gas side of nozzle assembly
in	inlet of flow stage
j	flow stage j
m	material
mom	momentum
out	outlet of flow stage
s	static conditions
sg	saturated gas phase
sl	saturated liquid phase
t	stagnation conditions
tot	total flow rate at nozzle coolant-tube inlet (eq. (1))
tp	two-phase flow
w	wall
τ_i	time at end of time period $\tau_i - \tau_{i-1}$
τ_{i-1}	time at beginning of time period $\tau_i - \tau_{i-1}$
τ_0	time zero
τ_1	end value of time period $\tau_i - \tau_{i-1}$
1	flow stage 1

APPENDIX B

DESCRIPTION OF NOZZLE ANALYTICAL CODE (NAC)

The Nozzle Analytical Code (NAC) was developed to analyze the pressure-drop - heat-transfer characteristics of the RN-2 regeneratively cooled nozzle assembly used in the B-1 engine system tests. The program is written in FORTRAN IV to be accepted by an IBM 7094 digital computer. Qualified requesters may obtain a FORTRAN listing of the NAC (which includes the subprograms and subroutines used in the code) from the authors.

The NAC FORTRAN code consists of the main program (NAC Program), five subprograms, and ten subroutines. Some of these subprograms and subroutines are of secondary significance and are used primarily as supplements to the major subprograms and subroutines in the code. A brief description of the NAC Program together with the major subprograms and subroutines follows.

NAC Program

The NAC program reads in and prepares the time-dependent input data to be used in the calculations. The program generates the required data pertinent to a particular run and sets up branches and indexes for the numerical operations.

GASFLO Subroutine

The GASFLO subroutine is used to calculate the static pressure drops, static pressures, and heat-transfer rates in each of the flow stages for gaseous-hydrogen flow conditions. Material temperatures, fluid temperatures, fluid velocities, Mach numbers, and coolant-side heat-transfer coefficients for the individual flow stages are also computed for each time period in this subroutine. The material temperatures calculated for a specific time period are used as input data for the succeeding time period.

TWOPHS Subroutine

The TWOPHS subroutine is used to calculate the static pressure drops, static pressures, and heat-transfer rates in each of the flow stages for two-phase and subcooled liquid-hydrogen flow conditions. The procedure used in the subroutine is essentially the same as that used in the GASFLO subroutine. The TWOPHS subroutine also computes

material temperatures, fluid temperatures, fluid qualities, fluid velocities, two-phase and subcooled-liquid Mach numbers, and coolant-side heat-transfer coefficients of the flow stages for each time period.

HOTGAS Subroutine

The HOTGAS subroutine calculates hot-gas-side heat-transfer coefficients and the rates of heat transfer from the hot gas side of the nozzle to the coolant-tube wall.

SOLVE Subroutine and MGAUSD Subroutine

The SOLVE and MGAUSD subroutines are used to calculate appropriate fluid temperatures and material temperatures that satisfy a particular series of iterative equations.

STATE Subroutine

The STATE subroutine calculates gaseous, two-phase, and liquid-hydrogen state relations, thermodynamic properties, and transport properties for any fixed ortho-para composition. The hydrogen properties used to obtain the calculated results in this report were based on an assumed composition of 97-percent para-hydrogen and 3-percent ortho-hydrogen. The STATE subroutine is described in reference 5.

CURVE Subprogram

The CURVE subprogram computes the specific heat of the nozzle materials (Inconel-X) from curve-fit equations of specific heat c_m as a function of the temperature. This subprogram contains data for temperatures ranging from approximately 30° to 600° R.

XTTCRV Subprogram

The XTTCRV subprogram is used to calculate the coefficient Φ_{tt} used in the two-phase-flow pressure-drop equation (see eq. (C19)). The coefficient Φ_{tt} is expressed as a function of $\sqrt{X_{tt}}$ by a polynominal curve-fit equation.

CRVXTT Subprogram

The CRVXTT subprogram is used to obtain the experimental Nusselt number Nu_{exp} for two-phase film-boiling heat transfer. The ratio Nu_{exp}/Nu_{cal} is expressed as a function of

$$\frac{1}{0.706 + 1.6\ X_{tt,f} - 0.123(X_{tt,f})^2}$$

by a curve-fit equation (see eq. (7)).

Input Data

The input data for the NAC is made up of three separate groups. The data for each of the three groups are described and discussed herein.

Group I, geometric input. - The geometric input group consists of a list of geometric constants that are assigned to each of the flow stages in the single-tube model. As mentioned in the ANALYTICAL PROCEDURE section, the single-tube flow model used in the NAC to represent the RN-2 nozzle assembly was divided into 32 axial segments (flow stages), each with a length of 2 inches. Flow stages 1 to 17 represent the major segment of the nozzle, which extends from the nozzle inlet manifold to the nozzle throat. Flow stages 18 to 32 represent the segment of the nozzle that extends from the nozzle throat to the coolant-tube outlet and is supported by the structural shell.

The geometric input data for the RN-2 nozzle assembly are listed in table I. As indicated in table I, the material weights and coolant-tube surface areas assigned to the flow stages in segment L_2 include values for both region A and region B of these flow stages. The material assigned to the separate regions (A and B) of these flow stages is as shown in figure 7 (p. 15).

For segment L_1, the coolant-tube average surface areas for heat transfer were computed as the product of the flow-stage length and the average flow-stage inside perimeter. The surface areas for the heat transfer from regions A and B of the flow stages in segment L_2 were computed as the product of the flow-stage length and the respective average inside surface perimeters.

The coolant-tube average hydraulic diameters for the individual flow stages were computed as the following:

$$\text{Average hydraulic diameter of flow stage} = \frac{4(\text{average flow area of flow stage})}{\text{average total perimeter of flow stage}} \qquad \text{(B1)}$$

TABLE I. - GEOMETRIC INPUT DATA FOR RN-2 NOZZLE ASSEMBLY

Flow stage	Weight of material assigned to flow stage, W_m, lb		Coolant-tube average hydraulic diameter, D, ft	Coolant-tube average surface area, A_s, ft^2		Single coolant-tube flow area, A, ft^2		Exhaust side average hydraulic diameter, d, in.	Exhaust side surface area for heat transfer, $A_{s,hs}$, ft^2
						Inlet	Outlet		
1	0.01153		0.0467	0.02490		0.00179	0.00170	29.60	0.00716
2	.01142		.0448	.02466		.00170	.00161	28.95	.00701
3	.01125		.0431	.02430		.00161	.00152	28.20	.00683
4	.01104		.0415	.02381		.00152	.00143	27.30	.00661
5	.01074		.0400	.02322		.00143	.00134	26.30	.00637
6	.01044		.0385	.02255		.00134	.00125	25.20	.00610
7	.01009		.0370	.02180		.00125	.00116	24.00	.00582
8	.00967		.0356	.02086		.00116	.00107	22.80	.00552
9	.00922		.0343	.01990		.00107	.00097	21.40	.00518
10	.00871		.0329	.01880		.00097	.00087	20.05	.00486
11	.00814		.0313	.01759		.00087	.00077	18.65	.00452
12	.00755		.0295	.01630		.00077	.00067	17.20	.00417
13	.00690		.0275	.01490		.00067	.00056	15.70	.00381
14	.00624		.0252	.01348		.00056	.00045	14.05	.00342
15	.00554		.0226	.01195		.00045	.00036	12.50	.00301
16	.00503		.0201	.01086		.00036	.00030	10.75	.00260
17	.00489		.0176	.01057		.00030	.00026	8.90	.00217
	Region A	Region B		Region A	Region B				
18	0.00458	0.00682	.0168	0.00988	0.00069	.00026	.00028	8.80	.00214
19	.00455	.00753	.0174	.00981	.00077	.00028	.00034	10.10	.00245
20	.00485	.00950	.0195	.01144	.00095	.00034	.00046	12.30	.00301
21	.00656	.01230	.0220	.01417	.00120	.00046	.00061	15.20	.00368
22	.00763	.01615	.0250	.01647	.00153	.00061	.00079	18.00	.00436
23	.00846	.02127	.0286	.01824	.00197	.00079	.00099	20.90	.00507
24	.00919	.02690	.0330	.01982	.00228	.00099	.00125	23.80	.00575
25	.00989	.02780	.0383	.02132	.00246	.00125	.00154	26.60	.00645
26	.01050	.02966	.0440	.02264	.00257	.00154	.00182	29.45	.00710
27	.01110	.03100	.0506	.02392	.00263	.00182	.00210	32.30	.00783
28	.01164	.03220	.0555	.02513	.00267	.00210	.00237	34.60	.00838
29	.01219	.03320	.0573	.02630	.00270	.00237	.00254	35.50	.00860
30	.01270	.03370	.0566	.02738	.00272	.00254	.00256	36.00	.00873
31	.01320	.03370	.0548	.02843	.00272	.00256	.00257	36.20	.00878
32	.01368	.03370	.0532	.02948	.00272	.00257	.00257	36.20	.00878

The average surface areas for heat transfer from the hot gas side of the nozzle were computed from

$$A_{s,hs} = \frac{\pi d l}{180} \tag{B2}$$

As pointed out in the ANALYTICAL PROCEDURE section, the effective surface areas for heat transfer to the flow stages from the hot gas side of the nozzle were based on the assumption that the inside surface of the RN-2 nozzle assembly was smooth. Because of the tubular wall construction, the actual surface areas for heat transfer of the flow stages from the hot gas side are somewhat larger than the values in table I.

Group II, fixed constants and functions. - The fixed constants and functions used in the NAC are listed and defined as follows:

$C_{(1-32)}$	values of the variable coefficient (eq. (9)) for flow stages 1 to 32. (Values of C used for individual flow stages are shown in fig. 9.)
g	conversion factor, 32.174 ft/sec^2
l	flow-stage length, ft
$\left(\mathscr{P}_s/\mathscr{P}_t\right)_{(1-32)}$	ratio of static to total pressure on hot gas side of nozzle for flow stages 1 to 32
R_g	specific gas law constant, 766 ft/$^\circ$R
$\left(T_{cs}/T_{ct}\right)_{(1-32)}$	ratio of static to total temperature on hot gas side of nozzle for flow stages 1 to 32
$T_{m,B,\tau_0}{}_{(18-32)}$	average material temperatures of region B for flow stages 18 to 32 at time τ_0, $^\circ$R
$T_{w,A,\tau_0}{}_{(18-32)}$	wall temperatures of region A for flow stages 18 to 32 at time τ_0, $^\circ$R
$T_{w,\tau_0}{}_{(1-17)}$	wall temperatures of flow stages 1 to 17 at time τ_0, $^\circ$R
T	total time span of test run under consideration, sec
$\tau_i - \tau_{i-1}$	time period used in the analysis, sec

Group III, time-dependent input. - The time-dependent input data used in the NAC are listed and defined as follows:

$P_{s,1,in}$	static pressure at the inlet to flow stage 1, psia
$\mathscr{P}_{s,in}$	static pressure on hot gas side of nozzle at nozzle chamber inlet, psia

$T_{b,1,in}$ fluid temperature at the inlet to flow stage 1, ^{o}R

T_{ct} fluid temperature on hot gas side of nozzle at nozzle chamber inlet, ^{o}R

$X_{1,in}$ fluid quality at inlet to flow stage 1, lb_{gas}/lb_{fluid}

$\dot{\omega}_{c}$ flow rate in a single RN-2 nozzle coolant tube, lb/sec

$\dot{\omega}_{hs}$ total flow rate on hot gas side of nozzle, lb/sec

The time-dependent input data used for liquid-hydrogen test run 24 are shown in figures 10 to 13 (pp. 26 to 28). The numerical values of the time-dependent data used in the NAC were taken at a mean value in each representative time period. For liquid-hydrogen test run 24, a time period of 0.1 second was used, and the numerical values of the time-dependent data were taken at each 0.1 second, starting at $\tau = 0.05$ second.

Output Data

The output from the NAC contains the following time-dependent data:

$h_{(1-17)}$ heat-transfer coefficient of inside coolant-tube surface for stages 1 to 17, $Btu/(sec)(^{o}R)(ft)^{2}$

$h_{A_{(18-32)}}$ heat-transfer coefficient from surface of region A in stages 18 to 32, $Btu/(sec)(^{o}R)(ft)^{2}$

$h_{B_{(18-32)}}$ heat-transfer coefficient from surface of region B in stages 18 to 32, $Btu/(sec)(^{o}R)(ft)^{2}$

$h_{hs_{(1-32)}}$ heat-transfer coefficient on hot side of nozzle for stages 1 to 32, $Btu/(sec)(^{o}R)(ft)^{2}$

$M_{out_{(1-32)}}$ Mach number at the outlet of flow stages 1 to 32

$P_{s,out_{(1-32)}}$ static pressure at the outlet of flow stages 1 to 32, psia

$\Delta P_{s_{(1-32)}}$ static pressure drop in each flow stage (stages 1 to 32), psi

$Q_{(1-32)}$ heat transferred from flow stages 1 to 32 in time period $\tau_{i} - \tau_{i-1}$, Btu per time period

$q_{(1-32)}$ heat transferred from hot gas side of nozzle to flow stages 1 to 32 in time period $\tau_{i} - \tau_{i-1}$, Btu per time period

$Re_{b_{(1-32)}}$	average Reynolds number (based on average hydraulic diameter and average flow area) of flow stages 1 to 32
$T_{b,out_{(1-32)}}$	fluid total temperature at outlet of flow stages 1 to 32, ^{o}R
$T_{m,B_{(18-32)}}$	average material temperature for region B of flow stages 18 to 32, ^{o}R
$T_{w_{(1-17)}}$	wall temperature of flow stages 1 to 17, ^{o}R
$T_{w,A_{(18-32)}}$	wall temperature for region A of flow stages 18 to 32, ^{o}R
$T_{w,B_{(18-32)}}$	wall temperature for region B of flow stages 18 to 32, ^{o}R
$v_{out_{(1-32)}}$	fluid average velocity at the outlet of flow stages 1 to 32, ft/sec

APPENDIX C

ANALYTICAL EQUATIONS AND ASSUMPTIONS

Heat-Transfer Equations

The initial assumptions used in the prediction of the pressure-drop - heat-transfer characteristics of the regeneratively cooled RN-2 nozzle assembly were described in the INTRODUCTION section of this report. In developing a heat balance around the individual flow stages of the single-tube flow model, the following additional assumptions were made:

(1) The single-tube flow rate $\dot{\omega}_c$ is constant along the length of the nozzle at each point in time throughout a test run; that is,

$$\left(\frac{\partial \dot{\omega}_c}{\partial x}\right)_{\tau_i - \tau_{i-1}} = 0$$

(2) The temperature gradient across the 0.009-inch-thick Inconel-X tube wall is negligible.

(3) The heat transferred by conduction along the length of the nozzle coolant tubes and the nozzle support shell is negligible.

(4) The heat transferred by conduction from the exterior nozzle hardware (i.e., the nozzle flange, the support bands, and the leak collector manifold) is negligible in comparison to the net heat transfer in the flow stages by forced convection.

These four assumptions were investigated analytically for the conditions anticipated in the nozzle assembly during a typical B-1 system chilldown test. The results of these investigations indicated that the aforementioned assumptions were reasonably valid.

As pointed out in the section ANALYTICAL PROCEDURE, the heat-transfer equations and the methods of solution employed in the analysis of the individual flow stages of the single-tube model are dependent on the type of flow (gas, two-phase or subcooled liquid flow) and the major segment of the nozzle (L_1 or L_2) being analyzed. The heat-balance equations used in the NAC to predict the transient chilldown characteristics of the flow stages in segments L_1 and L_2 are described below.

Segment L_1

A typical flow stage in segment L_1 is shown in figure 19(a). The heat exchange from the typical flow stage in segment L_1 (to which heat is added by convection from the

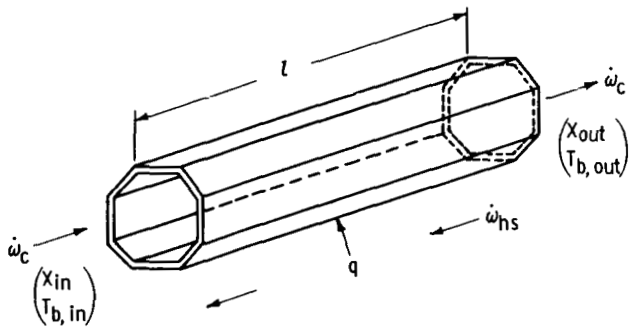

(a) Segment L_1.

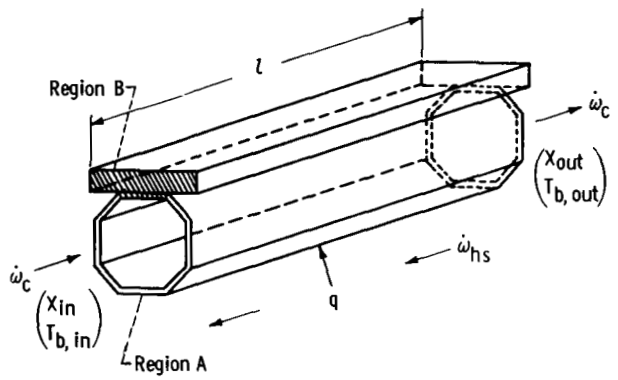

(b) Segment L_2.

Figure 19. - Typical flow stage in segments L_1 and L_2.

hot gas side of the nozzle and heat is removed by hydrogen flowing inside the coolant tubes) is calculated from the following equations.

Heat input to tube from hot side of nozzle in time period $\tau_i - \tau_{i-1}$:

$$q = h_{hs}A_{s,hs}\left(T_{cm} - T_{w,\tau_{i-1}}\right)(\tau_i - \tau_{i-1}) \tag{C1}$$

Heat transferred to coolant in time period $\tau_i - \tau_{i-1}$:

For $X = 1$ (gas flow) or $X = 0$ (subcooled liquid flow),

$$Q = \dot{\omega}_c c_{p,b}(T_{b,out} - T_{b,in})(\tau_i - \tau_{i-1}) \tag{C2}$$

For $0 < X < 1$ (two-phase flow),

$$Q = \dot{\omega}_c \lambda (X_{out} - X_{in})(\tau_i - \tau_{i-1}) \tag{C3}$$

Heat loss from coolant tube in time period $\tau_i - \tau_{i-1}$:

$$Q = hA_s\left(T_{w,\tau_{i-1}} - T_{b,in}\right)(\tau_i - \tau_{i-1}) \tag{C4}$$

Net heat loss from coolant tube in time period $\tau_i - \tau_{i-1}$:

$$Q = W_m c_m\left(T_{w,\tau_{i-1}} - T_{w,\tau_i}\right) + q \tag{C5}$$

The equation used to calculate the heat transferred to the coolant in the time period $\tau_i - \tau_{i-1}$ depends on the state of the hydrogen entering the flow stage. For gaseous flow or subcooled liquid flow, equation (C2) is used; for two-phase hydrogen flow ($0 < X < 1$), equation (C3) is used.

Equations (C1) to (C5) are solved simultaneously by an iterative procedure, and values are obtained for Q, q, $T_{b,out}$ (or X_{out}), and T_{w,τ_i}.

Segment L_2

Figure 19(b) shows a typical flow stage in segment L_2.

The heat transferred from a typical stage in segment L_2 is calculated from a heat balance around the two separate regions that make up the flow stage.

The heat-balance equations for region A of a typical flow stage in segment L_2 are as follows.

Heat input to region A from hot side of nozzle in time period $\tau_i - \tau_{i-1}$:

$$q = h_{hs}A_{s,hs}\left(T_{cm} - T_{w,A,\tau_{i-1}}\right)(\tau_i - \tau_{i-1}) \tag{C6}$$

Heat transferred to coolant from region A in time period $\tau_i - \tau_{i-1}$:

For $X = 1$ (gas flow) or $X = 0$ (subcooled liquid flow),

$$Q_A = \dot{\omega}_c c_{p,b}(T_{b,A,out} - T_{b,in})(\tau_i - \tau_{i-1}) \tag{C7}$$

For $0 < X < 1$ (two-phase flow),

$$Q_A = \dot{\omega}_c \lambda(X_{A,out} - X_{in})(\tau_i - \tau_{i-1}) \tag{C8}$$

Heat loss from region A material in time period $\tau_i - \tau_{i-1}$:

$$Q_A = h_A A_{s,A}\left(T_{w,A,\tau_{i-1}} - T_{b,in}\right)(\tau_i - \tau_{i-1}) \tag{C9}$$

Net heat transferred from region A material in time period $\tau_i - \tau_{i-1}$:

$$Q_A = W_{m,A}c_{m,A}\left(T_{w,A,\tau_{i-1}} - T_{w,A,\tau_i}\right) + q \tag{C10}$$

From an iterative solution of the heat-balance equations for region A of segment L_1 (eqs. (C6) to (C10)), the values for q, Q_A, $T_{b,A,out}$ or $X_{A,out}$, and T_{w,A,τ_i} are obtained. The calculated values of $T_{b,A,out}$ or $X_{A,out}$ are taken as the initial conditions for the calculations made on region B in the flow stage under consideration. In effect, regions A and B are considered to be arranged in series.

For region B of the typical flow stage under consideration, the heat-balance equations are as follows.

Heat loss from region B material in time period $\tau_i - \tau_{i-1}$:

$$Q_B = h_B A_{s,B}\left(T_{w,B,\tau_{i-1}} - T_{b,A,out}\right)(\tau_i - \tau_{i-1}) \tag{C11}$$

Heat loss from material in region B in time period $\tau_i - \tau_{i-1}$:

$$Q_B = W_{m,B} c_{m,B}\left(T_{m,B,\tau_{i-1}} - T_{m,B,\tau_i}\right) \tag{C12}$$

Heat transferred to coolant from region B in time period $\tau_i - \tau_{i-1}$:

For $X = 1$ (gas flow) or $X = 0$ (subcooled liquid flow),

$$Q_B = \dot{\omega}_c c_{p,b}\left(T_{b,out} - T_{b,A,out}\right)(\tau_i - \tau_{i-1}) \tag{C13}$$

For $0 < X < 1$ (two-phase flow),

$$Q_B = \dot{\omega}_c \lambda (X_{B,out} - X_{A,out})(\tau_i - \tau_{i-1}) \tag{C14}$$

Because of the significant thickness of the support shell on the RN-2 nozzle, the temperature gradient across the thickness of region B was found to be appreciable during a chilldown. In order to obtain a wall temperature for use in the succeeding time period, a relation between the region B average material temperature T_{m,B,τ_i} and the region B coolant-side wall temperature T_{w,B,τ_i} must be known. The temperature distributions resulting from several transient chilldown analyses of a typical flow stage in segment L_1 were determined using TOSS (ref. 18). For the transient conditions anticipated in the nozzle during a typical B-1 chilldown test, a simple, approximate relation was obtained, which relates the region B wall temperature T_{w,B,τ_i} to the region B average material temperature T_{m,B,τ_i} and the region A material temperature T_{w,A,τ_i}. This relation is as follows:

$$T_{w,B,\tau_i} = \frac{1}{2}\left(T_{m,B,\tau_i} + T_{w,A,\tau_i}\right) \tag{C15}$$

Equation (C15) along with equations (C11) to (C14) are solved in the NAC to obtain the values of Q_B, T_{w,B,τ_i}, $T_{b,out}$, and T_{m,B,τ_i} or $X_{B,out}$.

Pressure-Drop Equations

When changes in potential energy are neglected, the static pressure drop in a typical flow stage of the single-tube model is computed by adding the friction and momentum pressure drops; that is, the static pressure drop in a typical flow stage, for example, stage j, is given by

$$\Delta P_{s,j} = \Delta P_{fr,j} + \Delta P_{mom,j} \tag{C16}$$

For gas, two-phase, and subcooled liquid flow in the nozzle coolant tubes, the momentum pressure drop is given by the following relation:

$$\Delta P_{mom,j} = \frac{1}{144} \frac{\dot{\omega}_c^2}{g A_{j,av}} \left[\frac{1}{(\rho A)_{j,out}} - \frac{1}{(\rho A)_{j,in}} \right] \tag{C17}$$

The equations used to compute the friction pressure drop in the individual flow stages depend on the local state (quality) of the fluid in the nozzle coolant tubes.

For gas flow and subcooled liquid flow, the friction pressure drop is computed as follows:

$$\Delta P_{fr,j} = \frac{1}{144} \left[\frac{\dot{\omega}_c^2}{2g\rho_{av}(A_{j,av})^2} \right] \left(\frac{4f_j l}{D_{j,av}} \right) \tag{C18}$$

For two-phase flow ($0 < X < 1$), the friction pressure drop in the nozzle coolant tubes is calculated from the two-phase-flow pressure-drop equations described in reference 16. That is,

$$\Delta P_{fr,j} = \Phi_{tt}^2 \, \Delta P_{j,gas} \tag{C19}$$

The friction pressure drop due to flow of the gas phase only is given by

$$\Delta P_{j,gas} = \frac{1}{144} \left[\frac{(X_{j,av}\dot{\omega}_c)^2}{(\rho_{sg})(A_{j,av})^2} \right] \left(\frac{4f_j l}{D_{j,av}} \right) \tag{C20}$$

The modulus Φ_{tt} in equation (C19) is a function of the Martinelli-Nelson two-phase-flow parameter; that is

$$\Phi_{tt} = \Phi(\chi_{tt}) \tag{C21}$$

where

$$\chi_{tt} = \left(\frac{\rho_{sg}}{\rho_{sl}}\right)^{0.555} \left(\frac{\mu_{sl}}{\mu_{sg}}\right)^{0.111} \left(\frac{1 - X_j}{X_j}\right) \tag{C22}$$

Figure 20 shows the relation between the modulus Φ_{tt} and the parameter χ_{tt}. This relation was obtained from reference 16 and was approximated in the NAC by a polynomial equation.

The static pressure at the outlet of stage j is obtained by subtracting the static pressure drop in stage j from the inlet static pressure:

$$P_{s,j,out} = P_{s,j,in} - \Delta P_{s,j} \tag{C23}$$

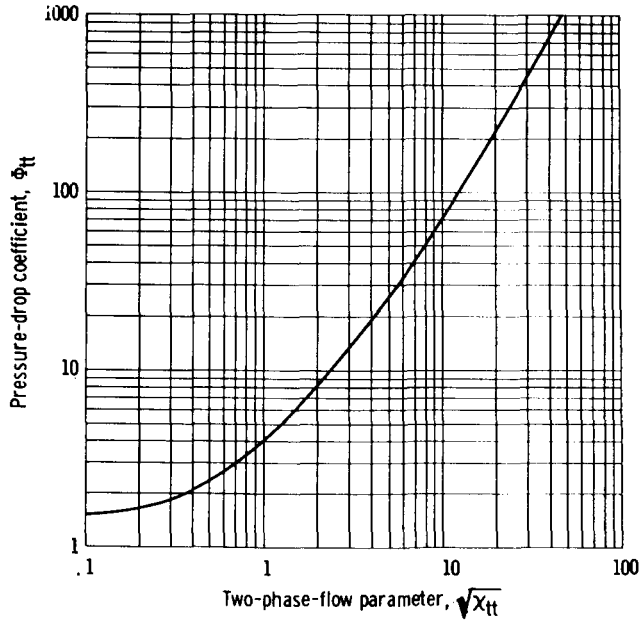

Figure 20. - Pressure-drop modulus as function of two-phase-flow parameter for flow mechanism in which both phases are in turbulent motion.

REFERENCES

1. Rostafinski, Wojciech; Rudey, Richard A.; Lacy, Donald D.; and Lillis, Patrick R.: Performance Characteristics of an Axial-Flow Liquid-Hydrogen Pump During Startup. NASA TM X-1213, 1965.

2. Clark, John S.: Analytical and Experimental Study of Startup Characteristics of a Full-Scale Unfueled Nuclear-Rocket-Core Assembly. NASA TM X-1231, 1966.

3. Straight, David M.; Biesiadny, Thomas A.; Pierce, John G.; and Metger, George W.: Component Flow and Fluid Properties During Cold Flow Experiments in a Nuclear Rocket System. NASA TM X-1366, 1966.

4. Lauritzen, John I., Jr.; Corruccini, Robert J.; and Lonberger, S. T.: Reference Tables for Thermocouples. Circular No. 561, NBS, Apr. 27, 1955.

5. Harry, David P., III: Formulation and Digital Coding of Approximate Hydrogen Properties for Application to Heat-Transfer and Fluid-Flow Computations. NASA TN D-1664, 1963.

6. Fowler, J. M.; and Warner, C. F.: Measurements of Heat Transfer Coefficients for Hydrogen Flowing in a Heated Tube. ARS J., vol. 30, no. 3, Mar. 1960, pp. 266-267.

7. Schlichting, Hermann (J. Kestin, trans.): Boundary Layer Theory. Fourth ed., McGraw-Hill Book Co., Inc., 1960.

8. Hines, W. S.; McCarthy, J. R.; Seader, J. D.; Trebes, D. M.; Gerstley, J. G.; Hodgdon, D. C.; Tobin, R. D.; and Wagner, W. R.: Investigation of Cooling Problems at High Chamber Pressures. Rep. No. R-3999 (NASA CR-50773), Rocketdyne Div. of North American Aviation, May 1963.

9. Wright, C. C.; and Walters, H. H.: Single Tube Heat Transfer Tests, Gaseous and Liquid Hydrogen. (WADC TR 59-423), AiResearch Mfg. Co., Aug. 1959.

10. Graham, Robert W.; Hendricks, Robert C.; and Ehlers, Robert C.: Analytical and Experimental Study of Pool Heating of Liquid Hydrogen Over a Range of Accelerations. NASA TN D-1883, 1965.

11. Hendricks, R. C.; Graham, R. W.; Hsu, Y. Y.; and Friedman, R.: Experimental Heat Transfer and Pressure Drop of Liquid Hydrogen Flowing Through a Heated Tube. NASA TN D-765, 1961.

12. Schacht, Ralph L.; Quentmeyer, Richard J.; and Jones, William L.: Experimental Investigation of Hot-Gas Side Heat-Transfer Rates for a Hydrogen-Oxygen Rocket. NASA TN D-2832, 1965.

13. Shapiro, Ascher H.: The Dynamics and Thermodynamics of Compressible Fluid Flow. Ronald Press Co., 1953.

14. Eckert, E. R. G.; and Drake, Robert M., Jr.: Heat and Mass Transfer. Second ed., McGraw-Hill Book Co., Inc., 1959.

15. McAdams, William H.: Heat Transmission. Third ed., McGraw-Hill Book Co., Inc., 1954.

16. Martinelli, R. C.; Boelter, L. M. K.; Taylor, T. H. M.; Thomsen, E. G.; and Morrin, E. H.: Isothermal Pressure Drop for Two-Phase Two-Component Flow in a Horizontal Pipe. ASME Trans., vol. 66, no. 2, Feb. 1944, pp. 139-151.

17. Hatch, M. R.; and Jacobs, R. B.: Prediction of Pressure Drop in Two-Phase Single-Component Fluid Flow. AICHE J., vol. 8, no. 1, Mar. 1962, pp. 18-25.

18. Bagwell, David: TØSS - An IBM-7090 Code for Computing Transient or Steady State Temperature Distributions. Report No. K-1494, Oak Ridge Gaseous Diffusion Plant, Dec. 1, 1961.

NASA-Langley, 1967 —— 28 E-3606